Petroleum Science 22 (2025) 1307–1339

Contents lists available at ScienceDirect

Petroleum Science

journal homepage: www.keaipublishing.com/en/journals/petroleum-science

Original Paper

Energy and heat transfer analysis on the heating process of crude oil tank with mechanical stirring

Jian Zhao [a], Ming-Yu Lei [a], Shu-Qi Liu [b], Hang Dong [a, *]

[a] Key Laboratory for Enhance Oil and Gas Recovery of the Ministry of Education, Northeast Petroleum University, Daqing, 163318, Heilongjiang, China
[b] Daqing Oilfield No. 4 Oil Production Plant, Daqing, 163318, Heilongjiang, China

ARTICLE INFO

Article history:
Received 15 April 2024
Received in revised form
5 August 2024
Accepted 21 December 2024
Available online 24 December 2024

Edited by Teng Zhu

Keywords:
Waxy crude oil
Mechanical stirring
Field synergy
Grey relational analysis
Multiple regression analysis
Entropy generation

ABSTRACT

Taking into account the characteristics of non-Newtonian fluids and the influence of latent heat of wax crystallization, this study establishes physical and mathematical models for the synergy of tubular heating and mechanical stirring during the waxy crude oil heating process. Numerical calculations are conducted using the sliding grid technique and FVM. The focus of this study is on the impact of stirring rate (τ), horizontal deflection angle (θ_1), vertical deflection angle (θ_2), and stirring diameter (D) on the heating effect of crude oil. Our results show that as τ increases from 200 rpm to 500 rpm and D increases from 400 mm to 600 mm, there is an improvement in the average crude oil temperature and temperature uniformity. Additionally, heating efficiency increases by 0.5% and 1%, while the volume of the low-temperature region decreases by 57.01 m^3 and 36.87 m^3, respectively. As θ_1 and θ_2 increase from 0° to 12°, the average crude oil temperature, temperature uniformity, and heating efficiency decrease, while the volume of the low-temperature region remains basically the same. Grey correlation analysis is used to rank the importance of stirring parameters in the following order: $\tau>\theta_1>\theta_2>D$. Subsequently, multiple regression analysis is used to quantitatively describe the relationship between different stirring parameters and heat transfer evaluation indices through equations. Finally, based on entropy generation minimization, the stirring parameters with optimal heat transfer performance are obtained when $\tau = 350$ rpm, $\theta_1 = \theta_2 = 0°$, and $D = 500$ mm.

1. Introduction

According to the BP Energy-Outlook 2023, global oil demand is projected to experience steady growth over the next decade. In the current complex international situation and background, ensuring adequate energy supply has become a top priority for most countries. In order to meet the domestic demand for crude oil consumption and ensure strategic reserves of crude oil, Chinese crude oil imports and reserves continue to grow (Wang et al., 2023). As one of the world's major suppliers and consumers of petroleum prodtucts, most of the crude oil produced in China is waxy crude oil (Zhao et al., 2022a), with high gel point and poor fluidity at low temperature (Souas et al., 2021). Crude oil storage tank is often adopted to store crude oil in practical engineering and ensure the continuity and reliability of crude oil supply. As primary equipment for storing crude oil, its safe operation is an important guarantee for the oil depot.

During the static cooling storage process of crude oil storage tanks, when the ambient temperature is low, the internal crude oil temperature field is uneven due to the heat dissipation of storage tanks to the external environment and the influence of natural convection in the tank (Mawire et al., 2013; Sun et al., 2018a; Zhao et al., 2019a). When the oil temperature continues to drop below the gel point, the crude oil would solidify and form a gelled oil layer around the tank (Zhao et al., 2019b), accelerating the corrosion of the metal materials in the tank (Fernandes et al., 2013). The uneven temperature field could make the distribution of gelled oil on the sidewall of tank irregular, and in serious cases, the gelled oil could affect the floating roof normal floating, causing floating roof's blockage and even capsizing. Meanwhile, if the gelled oil blocks the oil-inlet or oil-outlet in storage tank, it would affect the normal delivering and receiving operation in storage tank, causing a major accident. Therefore, in crude oil storage process in cold areas, to prevent the accident of condensation in storage tank or pipe due to the rapid cooling, heaters are usually used in practical engineering to maintain temperature and heat for large storage tank to ensure

* Corresponding author.
E-mail address: dh.123@163.com (H. Dong).

https://doi.org/10.1016/j.petsci.2024.12.020

crude oil with great fluidity. According to the existing heating methods, the tubular heater could effectively rise the overall temperature for storage tank and decrease the occurrence of condensation accidents (Wang et al., 2020a). Nevertheless, because of the limited natural convection, the uneven heating effect of the heater can still lead to an uneven temperature field distribution and the cold oil accumulates in some regions (Sun et al., 2016; Zhao et al., 2017a), forming local low temperature region and causing accidents. To relieve the problems such as uneven temperature field and low temperature danger region generated during the heating process in large crude oil storage tank, most of the tank are equipped with mechanical agitators inside in practical engineering. Zhao et al. (2023a, 2023b) studied the effect of mechanical stirring on crude oil velocity and temperature fields in the tank, proved that the effect of forced convection formed by stirring can greatly improve the fluidity of crude oil, strengthen the heat transfer between crude oil and make the crude oil temperature more uniform. Similarly, in other fields, many scholars (Chen et al., 2010; Du et al., 2013; Li et al., 2013, 2021a; Luo et al., 2020; Wang et al., 2020b) had also studied agitators and found that agitators can indeed make the velocity field evenly distributed, promote the full mixing of the medium, and improve temperature uniformity. Therefore, for large crude oil storage tank, the agitator could fully mix crude oil, so that the physical fields in storage tank are more uniform.

In the course of the previous research, our research group has studied the synergy of heating and stirring in the tank and found that the stirring can enhance heat transfer between crude oil, increase heating rate, and make crude oil temperature distribution more uniform (Zhao et al., 2023a, 2023b). However, there are many factors that affect the effect of stirring and uniformity of the internal physical fields, such as stirring rate (Scholz and Keck, 2015; Roldan-Cruz et al., 2021; Fang and Zou, 2022), stirring diameter (Zhang et al., 2018; Fang and Zou, 2022), deflection angle (Zhang et al., 2020a, 2021), etc. There is no systematic study for the effect of different stirring parameters on uniformity of the physical fields in crude oil storage tank, especially the effect of improvement on low-temperature region. Therefore, in this paper, on the basis of existing research work, based on the stirring rate (τ), horizontal deflection angle (θ_1), vertical deflection angle (θ_2) and stirring diameter (D) of the agitator, the variations in the chemical and physical properties of crude oil before and after the abnormal point temperature, as well as the influence of wax crystal precipitation on specific heat of crude oil during cooling process is considered, the heat transfer process under synergy of tubular heating and mechanical stirring is studied for different stirring parameters, the variations of flow and heat transfer in the central region of the tank and accident-prone low-temperature key region are focused on. Grey relational analysis, multiple regression analysis and entropy generation minimization are used to quantitatively represent the relationship between different stirring parameters and heat transfer evaluation indices, and stirring parameters for optimal heat transfer performance is obtained. The finding can serve as the theoretical foundation for structural design and optimization of the operating parameters of agitator and provide theoretical guidance for the formulation of mechanical stirring in actual crude oil storage tank.

Nomenclature

u	X-direction velocity component, m/s	h	Convective heat transfer coefficient, W/m$^2\cdot$°C
v	Y-direction velocity component, m/s	G_k	The generation of turbulence kinetic energy due to the mean velocity gradients
w	Z-direction velocity component, m/s	σ_k	The turbulent Prandtl number for turbulent kinetic energy k
λ	Thermal conductivity, W/m·°C	μ_t	Turbulent viscosity
T_o	Initial crude oil temperature, °C	R_{tank}	Radius of the computational domain, m
ρ	Density of crude oil, kg/m^3	σ_ε	The turbulent Prandtl number for turbulent dissipation rate ε
C_p	Specific heat of crude oil, J/Kg·°C	τ_0	Initial stirring rate, rpm
H_{tank}	Total height of the computational domain, m	τ	Stirring rate, rpm
Nu	Nusselt number		
Subscripts:			
sidewall	Sidewall of the tank	agitator	Agitator
basewall	Basewall of the tank	tube	Heating tube
topwall	Topwall of the tank	air	Atmospheric environment

2. Physical model

2.1. Computational domain

In this paper, the 1000 m^3 floating roof storage tank with agitator and heating tube is used as the study object to construct computational domain. To improve the efficiency of numerical calculation, the structure of floating roof storage tank in the actual project needs to be simplified. The process of simplification and related parameters of the model is described in authors' previous study (Zhao et al., 2023a), and the resulting computational domain is shown in Fig. 1.

The liquid level is 5 m, the diameter of the tank is 12 m in this paper, and the overall model is divided into static region and dynamic region, furthermore the dynamic region is the position where the agitator is located. The serpentine heating tube is used in static region, as shown in Fig. 1(b). In dynamic region, according the book (Chen, 1999), the stirring parameters are modeled by 1:1 size with three-bladed impeller, and the model of agitator is shown in Fig. 1(c) and (d). The specific parameters of heating tube and agitator have been described in the authors' previous study (Zhao et al., 2023b). In this paper to research the effect of stirring parameters on flow and heat transfer in storage tank, the horizontal deflection angle, vertical deflection angle and stirring diameter of the agitator are changed, as shown in Fig. 2.

2.2. Waxy crude oil

The waxy crude oil produced from Daqing Oilfield is used as research object, its microstructure and physical properties change significantly with the change in temperature (Chala et al., 2018; Zhao et al., 2021a, 2022b; Li et al., 2021b). The variation of the microstructure of waxy crude oil during cooling is shown in Fig. 3. Among them, the white part is wax crystal and the brown part is liquid hydrocarbon. When temperature is high enough, waxy crude oil is the single-phase system with great fluidity, as shown in Fig. 3(a). However, when the temperature drops below the wax appearance temperature, wax crystal begin to precipitate out of the

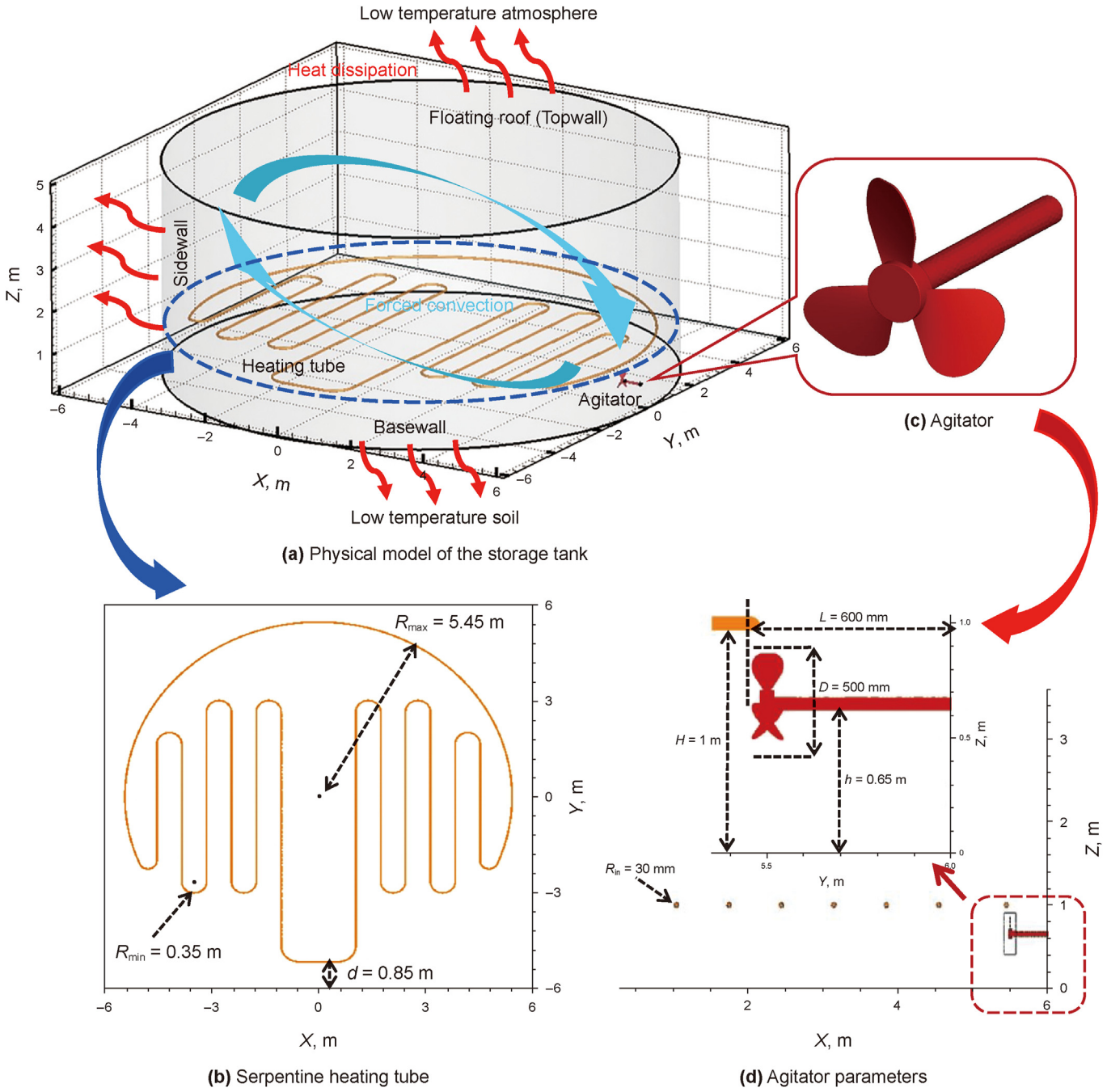

Fig. 1. Physical model.

system and grow gradually as the temperature decreases, which can be seen in Fig. 3(b). In this process, the latent heat released due to the wax crystal precipitation affects the specific heat capacity of crude oil. Meanwhile, wax crystal precipitation leads to a significant increase in the viscosity of waxy crude oil. As the temperature continues to decrease, wax crystal precipitates on a large scale, forming a three-dimensional mesh structure, as shown in Fig. 3(c). At this time, waxy crude oil can be seen as the porous medium system, where the wax crystal structure can be seen as a skeleton filled with liquid crude oil.

From the perspective of fluid properties, waxy crude oil is the Newtonian fluid when temperature exceeds the abnormal point temperature, and the relationship between viscosity and temperature is shown in Eq. (1). When crude oil temperature is below the abnormal point temperature, it is the non-Newtonian fluid, its viscosity is affected by temperature and shear rate, as shown in Eq. (2). Based on the experimental results shown in Fig. 4 from DSC (Differential Scanning Calorimetry), the latent heat generated by the precipitation of wax crystal could lead to an obvious variation in the specific heat capacity of waxy crude oil. In order to truly reflect the influence of latent heat on the specific heat capacity of the whole crude oil during the precipitation of wax crystal, the latent heat released by the precipitation of wax crystal is reflected on the change of the specific heat capacity of the overall crude oil. Therefore, the additional specific heat capacity method is adopted to represent the latent heat associated with wax crystal,

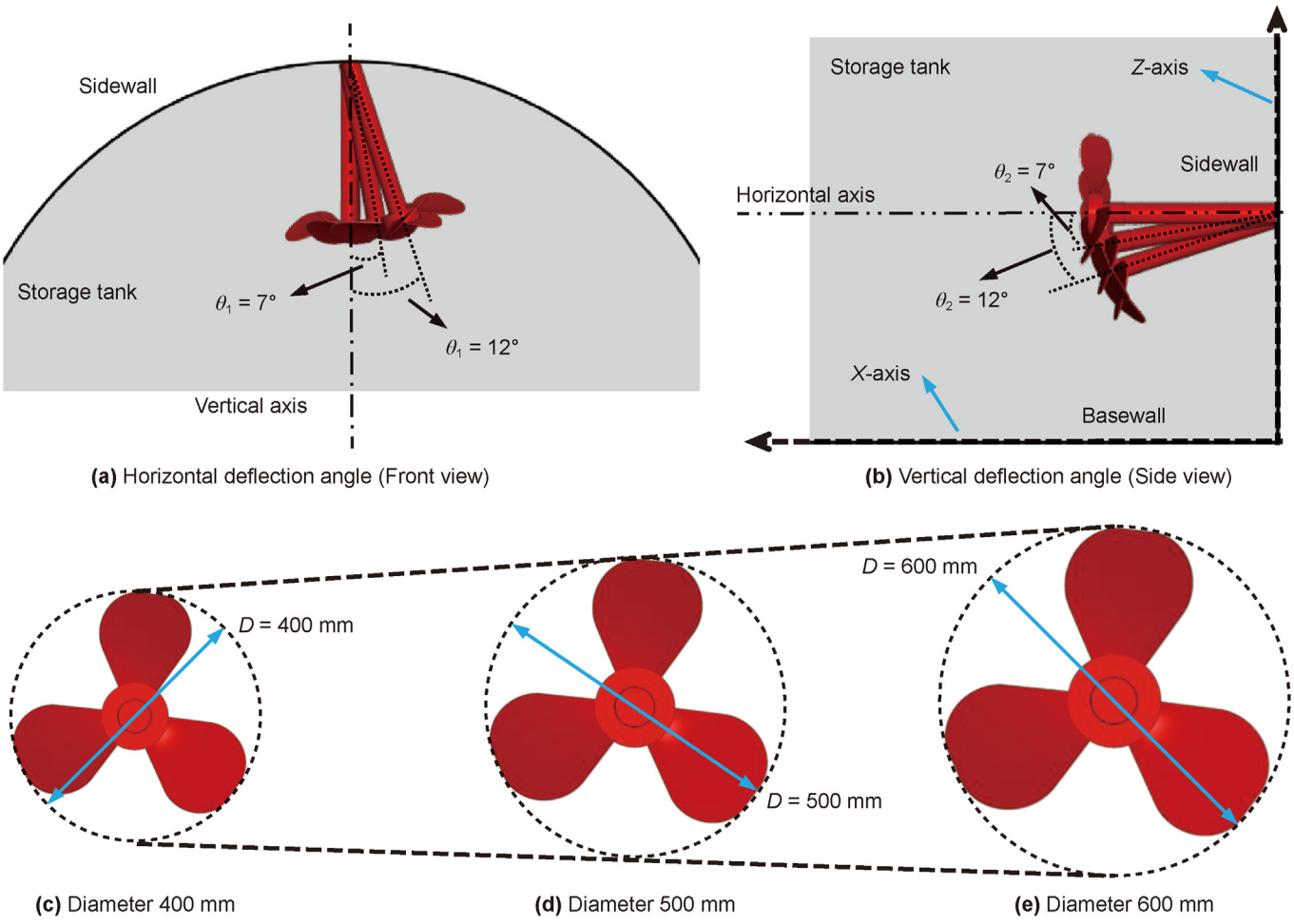

Fig. 2. Schematic diagram of stirring parameters.

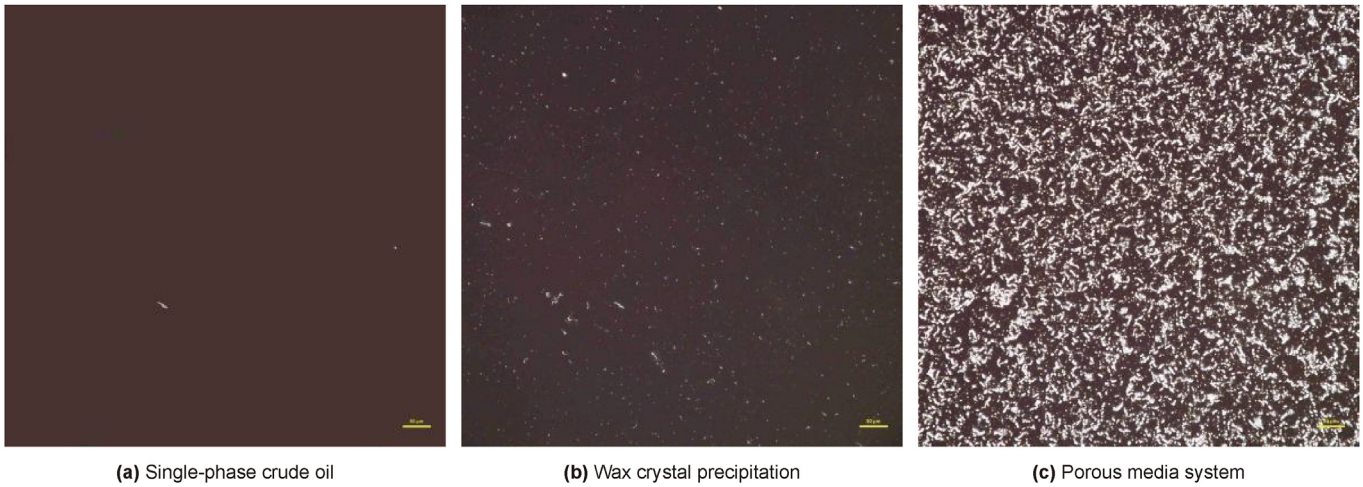

Fig. 3. Evolution of crude oil microstructure in the process of cooling.

the relationship between specific heat capacity and temperature is shown in Eq. (3). And the change in density of crude oil is considered in the buoyancy term for momentum equation, and the density is treated with Boussinesq approximation (Zhao et al., 2023b), as shown in Eq. (4).

$$\mu = 34866.25235 \times e^{-0.10368 \times T_{oil}}, T_{oil} > 35\ ^{\circ}C \quad (1)$$

$$\mu = e^{10.88837 - 0.08367 \times T_{oil}} \times \gamma^{-0.1608 - 0.00325 \times T_{oil}}, T_{oil} \le 35\ ^{\circ}C \quad (2)$$

where μ is the dynamic viscosity, mPa·s. γ is the shear rate, s^{-1}. T_{oil} is crude oil temperature, °C.

$$C_p = A + BT_{oil} + C{T_{oil}}^2 + D{T_{oil}}^3 + E{T_{oil}}^4 + F{T_{oil}}^5, T_{oil} > 25\ ^{\circ}C \quad (3)$$

The values of *A*-*F* are 2.5834, −0.0441, 0.0007, -4×10^{-6}, 1×10^{-8}, -1×10^{-11}, respectively.

$$\rho = \rho_{20} \times (1 - \beta \times (T_{oil} - 20)) \quad (4)$$

where ρ is the density of crude oil at, kg/m^3. β is the thermal expansion coefficient 0.000844 for crude oil. ρ_{20} is 855 kg/m^3 at 20 °C.

3. Mathematical models, validation and numerical approach

3.1. Mathematical models

3.1.1. Governing equations

The flow of crude oil in heating process is intense under stirring, and the governing equations need to be given (Seddegh et al., 2015; Mao et al., 2016).

(1) Continuity equation:

$$\frac{\partial \rho}{\partial t} + \frac{\partial(\rho u)}{\partial x} + \frac{\partial(\rho v)}{\partial y} + \frac{\partial(\rho w)}{\partial z} = 0 \quad (5)$$

(2) Momentum equation:

$$\frac{\partial(\rho u)}{\partial t} + \frac{\partial(\rho uu)}{\partial x} + \frac{\partial(\rho uv)}{\partial y} + \frac{\partial(\rho uw)}{\partial z} = \frac{\partial}{\partial x}\left((\mu+\mu_t)\frac{\partial u}{\partial x}\right) + \frac{\partial}{\partial y}\left((\mu+\mu_t)\frac{\partial u}{\partial y}\right) + \frac{\partial}{\partial z}\left((\mu+\mu_t)\frac{\partial u}{\partial z}\right) - \frac{\partial P}{\partial x} + \frac{\partial}{\partial x}\left((\mu+\mu_t)\frac{\partial u}{\partial x}\right) + \frac{\partial}{\partial y}\left((\mu+\mu_t)\frac{\partial v}{\partial x}\right) + \frac{\partial}{\partial z}\left((\mu+\mu_t)\frac{\partial w}{\partial x}\right) \quad (6)$$

$$\frac{\partial(\rho v)}{\partial t} + \frac{\partial(\rho vu)}{\partial x} + \frac{\partial(\rho vv)}{\partial y} + \frac{\partial(\rho vw)}{\partial z} = \frac{\partial}{\partial x}\left((\mu+\mu_t)\frac{\partial v}{\partial x}\right) + \frac{\partial}{\partial y}\left((\mu+\mu_t)\frac{\partial v}{\partial y}\right) + \frac{\partial}{\partial z}\left((\mu+\mu_t)\frac{\partial v}{\partial z}\right) - \frac{\partial P}{\partial y} + \frac{\partial}{\partial x}\left((\mu+\mu_t)\frac{\partial u}{\partial y}\right) + \frac{\partial}{\partial y}\left((\mu+\mu_t)\frac{\partial v}{\partial y}\right) + \frac{\partial}{\partial z}\left((\mu+\mu_t)\frac{\partial w}{\partial y}\right) \quad (7)$$

$$\frac{\partial(\rho w)}{\partial t} + \frac{\partial(\rho wu)}{\partial x} + \frac{\partial(\rho wv)}{\partial y} + \frac{\partial(\rho ww)}{\partial z} = \frac{\partial}{\partial x}\left((\mu+\mu_t)\frac{\partial w}{\partial x}\right) + \frac{\partial}{\partial y}\left((\mu+\mu_t)\frac{\partial w}{\partial y}\right) + \frac{\partial}{\partial z}\left((\mu+\mu_t)\frac{\partial w}{\partial z}\right) - \frac{\partial P}{\partial z} + \frac{\partial}{\partial x}\left((\mu+\mu_t)\frac{\partial u}{\partial z}\right) + \frac{\partial}{\partial y}\left((\mu+\mu_t)\frac{\partial v}{\partial z}\right) + \frac{\partial}{\partial z}\left((\mu+\mu_t)\frac{\partial w}{\partial z}\right) - \rho_{20}(1-\beta(T_{oil}-20))g \quad (8)$$

(3) Energy equation:

$$\frac{\partial(\rho T_{oil})}{\partial t} + \frac{\partial(\rho uT_{oil})}{\partial x} + \frac{\partial(\rho vT_{oil})}{\partial y} + \frac{\partial(\rho wT_{oil})}{\partial z} = \frac{\partial}{\partial x}\left(\frac{\mu}{Pr_t}\frac{\partial T}{\partial x}\right) + \frac{\partial}{\partial y}\left(\frac{\mu}{Pr_t}\frac{\partial T}{\partial y}\right) + \frac{\partial}{\partial z}\left(\frac{\mu}{Pr_t}\frac{\partial T}{\partial z}\right) \quad (9)$$

(4) Standard $k-\varepsilon$ equations:

$$\frac{\partial}{\partial t}(\rho k) + \frac{\partial}{\partial x}(\rho uk) + \frac{\partial}{\partial y}(\rho vk) + \frac{\partial}{\partial z}(\rho wk) = \frac{\partial}{\partial x}\left[\left(\mu + \frac{\mu_t}{\sigma_k}\right)\frac{\partial k}{\partial x}\right] + \frac{\partial}{\partial y}\left[\left(\mu + \frac{\mu_t}{\sigma_k}\right)\frac{\partial k}{\partial y}\right] + \frac{\partial}{\partial z}\left[\left(\mu + \frac{\mu_t}{\sigma_k}\right)\frac{\partial k}{\partial z}\right] + G_k - \rho\varepsilon \quad (10)$$

$$\frac{\partial}{\partial t}(\rho\varepsilon) + \frac{\partial}{\partial x}(\rho u\varepsilon) + \frac{\partial}{\partial y}(\rho v\varepsilon) + \frac{\partial}{\partial z}(\rho w\varepsilon) = \frac{\partial}{\partial x}\left[\left(\mu + \frac{\mu_t}{\sigma_\varepsilon}\right)\frac{\partial \varepsilon}{\partial x}\right] + \frac{\partial}{\partial y}\left[\left(\mu + \frac{\mu_t}{\sigma_\varepsilon}\right)\frac{\partial \varepsilon}{\partial y}\right] + \frac{\partial}{\partial z}\left[\left(\mu + \frac{\mu_t}{\sigma_\varepsilon}\right)\frac{\partial \varepsilon}{\partial z}\right] + C_{1\varepsilon}\frac{\varepsilon}{k}G_k - C_{2\varepsilon}\rho\frac{\varepsilon^2}{k} \quad (11)$$

The formula of μ_t is as follows:

$$\mu_t = \rho C_\mu \frac{k^2}{\varepsilon} \quad (12)$$

3.1.2. Boundary condition

The topwall and sidewall of the tank are the third boundary condition, the ambient temperature under simulated conditions is −20 °C. The basewall of the tank is adjacent to the soil, and the soil is considered as a constant temperature layer with a certain temperature and thickness, considering the thermal resistance of the soil (Wang et al., 2017; Zhao et al., 2017a):

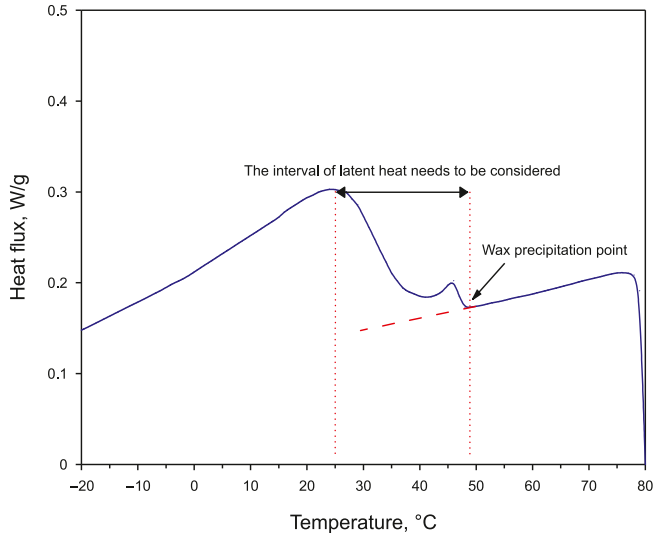

Fig. 4. Thermal characteristic curve of wax precipitation.

$$z = H_{\text{tank}}, 0 \le \sqrt{x^2 + y^2} \le R_{\text{tank}}, -\lambda_{\text{topwall}} \frac{\partial T_{\text{topwall}}}{\partial z} = h_{\text{topwall}} \left(T_{\text{topwall}} - T_{\text{air}} \right), u = v = w = 0 \tag{13}$$

$$0 \le z \le H_{\text{tank}}, \sqrt{x^2 + y^2} = R_{\text{tank}}, -\lambda_{\text{sidewall}} \left(\frac{\partial T_{\text{sidewall}}}{\partial x} + \frac{\partial T_{\text{sidewall}}}{\partial y} \right) = h_{\text{sidewall}} (T_{\text{sidewall}} - T_{\text{air}}), u = v = w = 0 \tag{14}$$

$$z = 0, 0 \le \sqrt{x^2 + y^2} \le R_{\text{tank}}, T_{\text{basewall}} = T_{\text{soil}}, u = v = w = 0 \tag{15}$$

The agitator is used to stir crude oil and its boundary condition are as follows:

$$-\lambda_{\text{agitator}} \left(\frac{\partial T_{\text{agitator}}}{\partial x} + \frac{\partial T_{\text{agitator}}}{\partial y} + \frac{\partial T_{\text{agitator}}}{\partial z} \right) = 0, \tau_{\text{agitator}} = \tau_0 \tag{16}$$

The heating tube is set as the first boundary condition:

$$T_{\text{tube}} = T_{\text{heat}} \tag{17}$$

Boundary conditions of the turbulent dissipation rate ε and the turbulent kinetic energy k:

$$\varepsilon = \frac{C_{\mu}^{\frac{3}{4}} k_p^{\frac{3}{2}}}{\kappa \Delta y_p} \tag{18}$$

$$k = \frac{3}{2} (\overline{V} \cdot I)^2 \tag{19}$$

where κ is Karman constant. I is the turbulence intensity. Δy_p is the distance from grid node P to the wall, m. $\overline{V}$ is the average velocity, m/s.

3.1.3. Initial condition

In the initial state, crude oil temperature is uniform and crude oil remains still in the tank.

$$T_{\text{oil}}(t = 0, x, y, z) = T_0, u = v = w = 0 \tag{20}$$

3.1.4. Evaluation indices in the process of flow and heat transfer

In the part of results and discussion, Pressure-Velocity synergy angle (β) (Liu et al., 2012), temperature variance (σ^2) and heating efficiency of the heater (η) are used as the evaluation indices in the numerical simulation heat transfer processes, and their expressions are as follows:

$$\beta = \arccos \frac{U \cdot (-\nabla p)}{|U||-\nabla p|} \tag{21}$$

$$\sigma^2 = \frac{\sum_{i=1}^{n} V_i (T_i - \overline{T})^2}{V} \tag{22}$$

$$\eta = \frac{Q_{\text{o}}}{Q_{\text{h}}} \tag{23}$$

where $U \cdot (-\nabla p)$ is the power of the fluid, which is the sum of the rate in kinetic energy loss and the power of viscous dissipation of crude oil. $|U||-\nabla p|$ is the total amount of power expended for the agitator to transfer momentum to the fluid. V_i, T_i are the volume and temperature of the ith grid, respectively. Q_{o}, Q_{h} are the heat for heating up the crude oil and the heat provided from heating tube.

3.2. Numerical approach

3.2.1. Discretization for the computational domain and validation for grid system

Firstly, the computational domain needs to be discretized. The computational domain is divided into two regions, the region including agitator is defined as the dynamic region, and the rest computational domain is defined as the static region. For the dynamic region, the minimum and maximum grid size are 3 mm and 12 mm, respectively, and the growth rate is 1.2. For the static region, the minimum and maximum grid size are 10 mm and 350 mm, respectively, and the growth rate is 1.2.

Subsequently, in order to verify the independence of the grid and reduce the influence of different grid size on the calculation results as much as possible. Based on the same model, four grid systems of different grid size are designed. The different grid systems and the simulation comparison results are shown in Table 1 and Fig. 5. Based on the comparison results, taking into account the calculation efficiency and accuracy, the optimal grid system Grid 3 under synergy of tubular heating and stirring is obtained, the details of the grid are shown in Fig. 6. The final number of grids is 2360432, and the method of discretization is appropriate, which can then be used for discretization with different stirring parameters (Zhao et al., 2023b).

3.2.2. Discretization for the governing equations

Based on the numerical calculation grid system designed, the computational domain is discretized into a large number of grids. The finite volume method is used to discretize the control equations for each grid. Considering the effect of buoyancy formed by convection, the Body Force weighted scheme is used to discretized the pressure. For the transient terms, the fully implicit first order temporal differentiation is used. The convective terms are treated with the second-order upwind scheme, and the diffusive terms are handled with central difference scheme. To accurately represent the pressure field, the staggered grid strategy is employed, with

Table 1
Different grid design schemes.

Grid	Minimum grid size, mm	Maximum grid size, mm	Growth rate	The number of grids	Calculate cost about 1 min, h
1	5	500	1.2	1675426	2.96
2	4.5	450	1.2	1848802	3.24
3	3	350	1.2	2360432	3.56
4	1.5	200	1.2	3318862	4.83

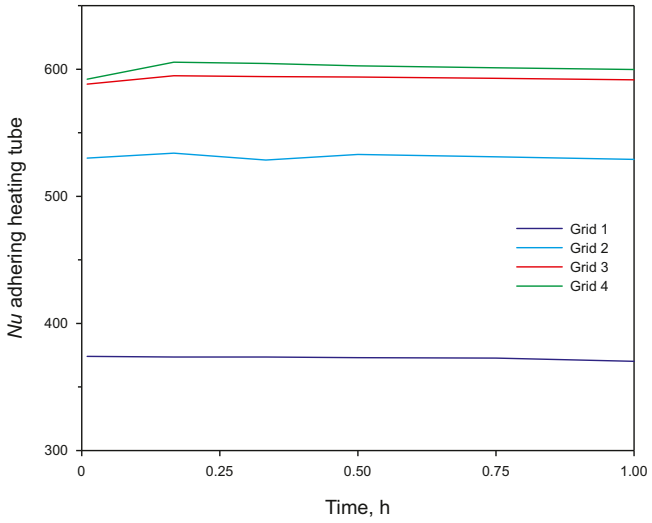

Fig. 5. Average *Nu* near heating tube.

velocity components and scalars stored in the grid strategy. Furthermore, to enhance the efficiency of the pressure-velocity coupling calculation, the SIMPLE algorithm is used to solve the pressure-velocity coupling problem and improves the efficiency of coupling calculation.

3.3. Validation for numerical approach

3.3.1. Comparison of small experimental tank

In order to ensure the accuracy of the simulation results, mathematical models, grid strategy and algorithm adopted in numerical simulation need to be validated before the numerical calculation. However, due to the high volume of the actual storage tank, and it is very difficult to make an experimental model with the same size as the actual storage tank for validation of numerical approach. Therefore, authors' group previously made a small experimental tank for experiment to compare the simulation results for the small experimental tank with the experimental results, and realized the validation for mathematical models, grid strategy and algorithm adopted in simulation (Zhao et al., 2023a, 2023b; Lei et al., 2024). For experimental conditions, the experimental environment is 10 °C, the initial temperature of the small experimental tank is 38 °C, the diameter of the small experimental tank is 80 cm, the liquid level height is 30 cm, the stirring rate is 50 rpm. So the same experiment equipment are used for the experiment and compared with numerical simulation result to validate the mathematical models, grid strategy and algorithm adopted in the simulation. The experiment equipment is shown in Fig. 7.

For the simulation, the same physical model as the small experimental tank was built and corresponding numerical simulation according to the experimental conditions of the small experimental tank was carried out. The parameter settings of numerical simulation is shown in Table 2. For the experiment, in order to ensure that the experimental results of the small experimental tank can be fully compared with the numerical simulation results, 12 thermocouple temperature sensors are arranged in the small experimental tank, which are used to measure the change of temperature. It can be seen from Table 3 and Fig. 8 that the temperature measured by the sensor in the small experimental tank is basically consistent with the temperature obtained by numerical simulation at the same position during the stirring process, and the relative error are within 3%. At the same time, in order to validate the accuracy of flow field results, the PIV system is introduced into the experiment equipment to measure the change of flow field in certain area near the agitator during stirring process. The comparison results of the velocity field in this area are shown in Fig. 9. Fig. 9 shows the numerical simulation and experimental results of the velocity change near the agitator, it can be seen that the relative errors between the simulation and experimental result are within 15%. The accuracy of mathematical models, grid strategy and algorithm adopted is validated and they are suitable for numerical simulation by comprehensively comparing the temperature and flow field results.

3.3.2. Comparison of actual large storage tank

The accuracy of mathematical models, grid strategy and algorithm can be proved by the validation with the small experimental tank. But in order to further validate whether the whole set of simulation method can meet the calculation accuracy when the size of the storage tank increases, the crude oil temperature data that authors' group measured previously on the actual 10^5 m^3 storage tank are used, the lay out of test tubes is shown in Fig. 10 (Yang et al., 2018). At the same time, for numerical simulation, the physical model that is the same as the actual 10^5 m^3 storage tank is established. According to the above mathematical models, grid strategy and algorithm, numerical calculation under the same conditions as the actual situation was carried out. The simulation results are compared with temperature measuring results, so as to prove the applicability of the simulation method for the large storage tank, and the comparison results are shown in Fig. 11. It can be seen from the figure that the temperature change trend of crude oil at different heights in the center of the tank is basically the same, and the maximum relative error of simulation and temperature measuring results is 7.64%, the minimum relative error is 2.85% and the average relative error is 4.92%. Adopting the same simulation method, the relative error between the numerical simulation and temperature measuring results increases when the size of storage tank increases. However, for 10^5 m^3 large storage tank, the relative error between simulation and measured results is still within 10%, and the result also has high accuracy. The comparison result of the small experimental tank and comparison result of the actual large storage tank demonstrate that the accuracy of the model, grid strategy and algorithm can be applied in subsequent simulation.

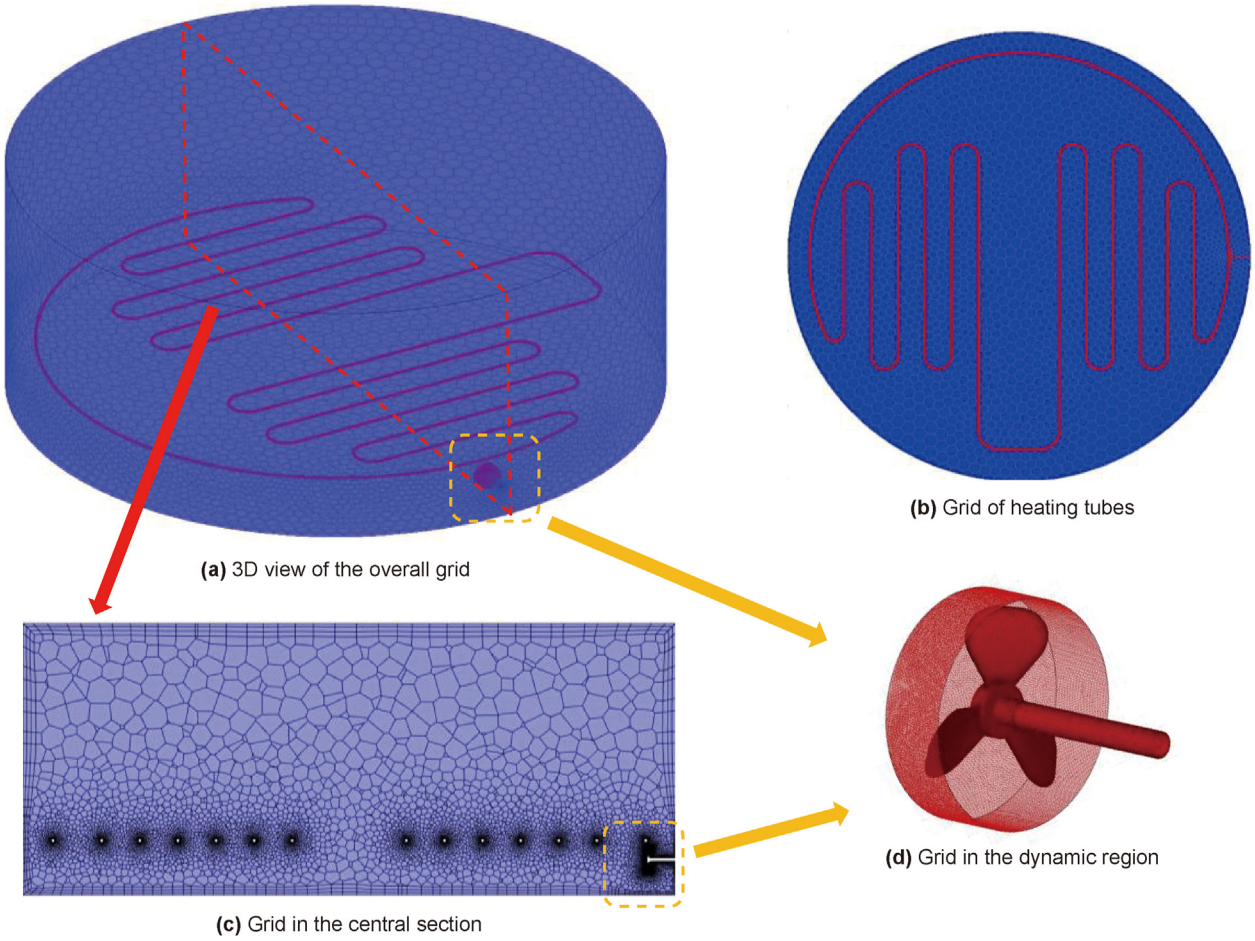

Fig. 6. Schematic of grid system.

4. Results and discussion

4.1. Simulation cases

According to the established physical model, the numerical simulation of heat transfer process for the crude oil under synergy of heating and stirring is carried out. For heating tube in actual storage tank, the velocity of medium in it is usually increased to maintain a constant wall temperature and heating efficiency. Considering the temperature range of the heating tube in the actual storage tank and research of some scholars (Sun et al., 2016; Zhang et al., 2020a), therefore, the heating tube is defined as a constant temperature of 80 °C. Based on different stirring parameters, all cases are designed, among which case 1 is the typical case. The main parameters in the cases are shown in Table 4.

4.2. Effect of different stirring parameters on the heat transfer and flow of crude oil

In order to explore the influence of different stirring parameters on the heating process under the synergy of stirring and tubular heating, variation law of the three-dimensional temperature and velocity fields in the central region of storage tank, the difference in distribution of temperature and velocity fields in the key sections, and temperature field in key region in the storage tank are analyzed in detail.

4.2.1. Stirring rate of agitator

(1) Effect of stirring rate on central region in storage tank

The temperature and velocity fields after 2 h of heating at different τ are shown in Fig. 12. Comparing the temperature and velocity contours in Fig. 12, it is evident that an increase in τ leads to a higher overall velocity, a more regular distribution of the velocity field, and a wider influence range of the agitator. The impact flow formed from mechanical stirring changes the direction of heat release by heating tube from natural convection to impact flow along the agitator. This phenomenon becomes more pronounced with larger values of τ, resulting in changes in temperature distribution. As τ increases, both the overall temperature and uniformity of the temperature field increase. Initially located near boundaries, particularly within low temperature regions at junctions between different boundaries, the impact on these regions is enhanced by the impact of agitator-driven velocity field as τ increases, leading to the increase in temperature and decrease in coverage within these regions. Simultaneously, strong impact flows weaken high temperature regions close to heaters. Consequently, stirring promotes a more uniform distribution for overall temperature. For sections $X = -4.8$ m, -1.6 m, 1.6 m and 4.8 m, the impact flow generated by the agitator takes away a amount of heat, which leads to a higher temperature in the region away from the agitator. Compared with average temperature in all four sections, $X = -4.8$ m is consistently highest while $X = 4.8$ m is consistently lowest for varying values of τ. The difference between $X = \pm 4.8$ m increases from 0.01 °C to 0.07 °C as τ increases from 200 rpm to 500 rpm. The results indicate

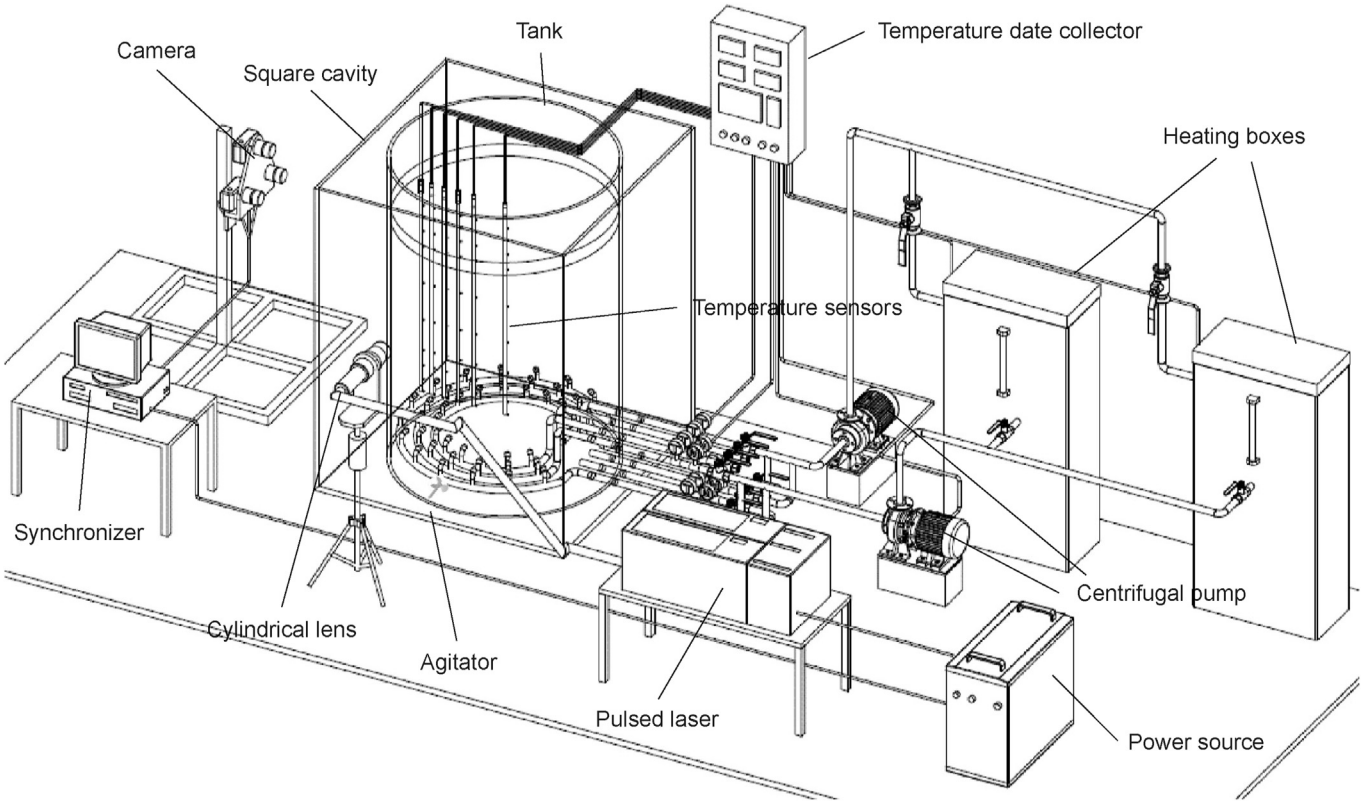

Fig. 7. Experiment equipment.

Table 2
Simulation parameters corresponding to small experimental tank.

Ambient temperature	Initial temperature	Diameter of tank	Liquid level	Stirring rate	Number of grids
10 °C	38 °C	80 cm	30 cm	50 rpm	389264

Table 3
The relative error of temperature in experiment and the numerical simulation.

Height from the bottom, cm	Relative error (Distance = 70 mm)	Relative error (Distance = 200 mm)	Relative error (Distance = 400 mm)	Relative error (Distance = 600 mm)
10	1.63%	2.53%	1.69%	2.02%
60	1.21%	0.96%	1.60%	1.04%
170	1.72%	1.77%	1.15%	0.55%

that an increase in τ leads to higher average temperature within each section along the direction of impact flow, as well as greater temperature variations between different sections. This observation is also evident from the contours shown in Fig. 13.

The strong impact flow carries a significant amount of heat to the boundary on the opposite side of the agitator, as shown in Fig. 13. This heat is then transferred upward along the side boundary, hindered by the upper boundary, and subsequently redirected backward along the upper boundary to form a vortex. As τ increases, the coverage of this vortex expands and eventually returns to a region near the agitator, forming a closed vortex. The presence of this vortex significantly influences the distribution of crude oil temperature, resulting in more intense heat transfer and higher temperature within its covered region compared to other areas. Conversely, regions unaffected by this vortex exhibit lower temperature and are more prone to forming low temperature regions at boundaries. Furthermore, upon comparing Fig. 13(a)–(c), it can be observed that an increase in τ from 200 rpm to 350 rpm leads to an expansion in the range of low temperature regions at boundary junctions. This phenomenon can be explained by Fig. 13(d)–(f). At slower τ, the vortex formed by stirring at the center covers a small area, the velocity at the boundary junction is less affected by it and other small vortices are spontaneously formed, which promotes the flow and heat transfer. However, when τ is 350 rpm, the coverage of the vortex at the center increases, the velocity field at the boundary junction is significantly affected by the vortex and the temperature decreases accordingly. Moreover, as τ further increases up to 500 rpm, the coverage of the vortex is further increased and a reverse vortex is induced at the boundary junction, which again promotes the heat transfer in this region and decreases the coverage of the low temperature region. Overall, increasing τ has a direct and pronounced effect on velocity and temperature fields near lower boundaries with rising temperature trends accompanied by faster rate. Therefore, the temperature and

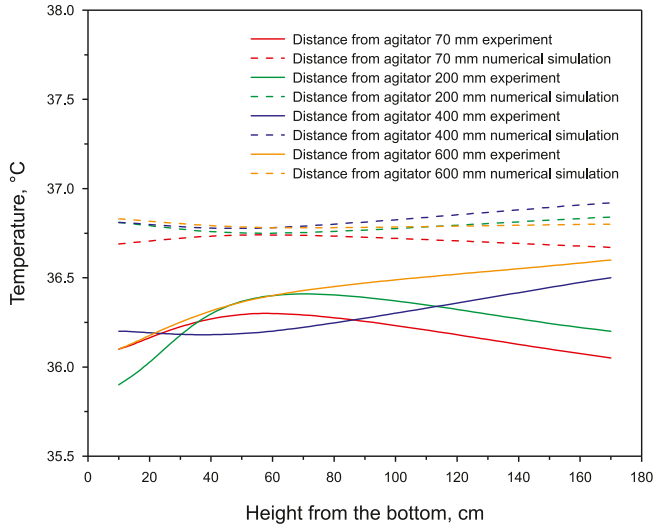

Fig. 8. Temperature comparison result.

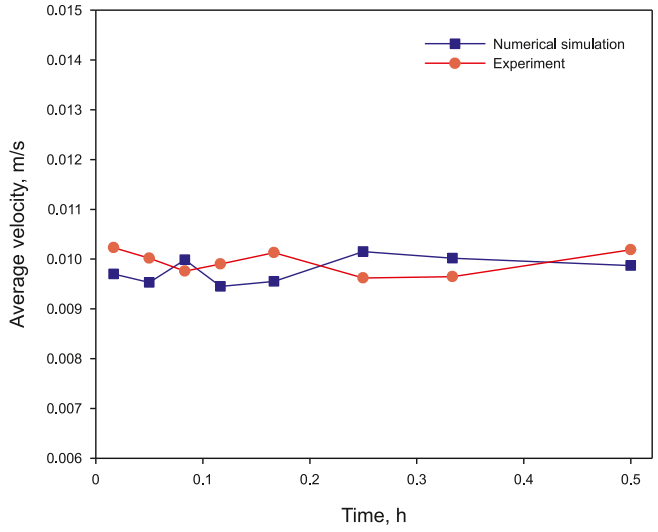

Fig. 9. Comparison of the velocity field near the agitator.

velocity in the vicinity of the lower boundary are given. As shown in Fig. 14(a)–(f), $Z = 0.65$ m represents the section where the agitator is positioned. It demonstrates that there still exist significant

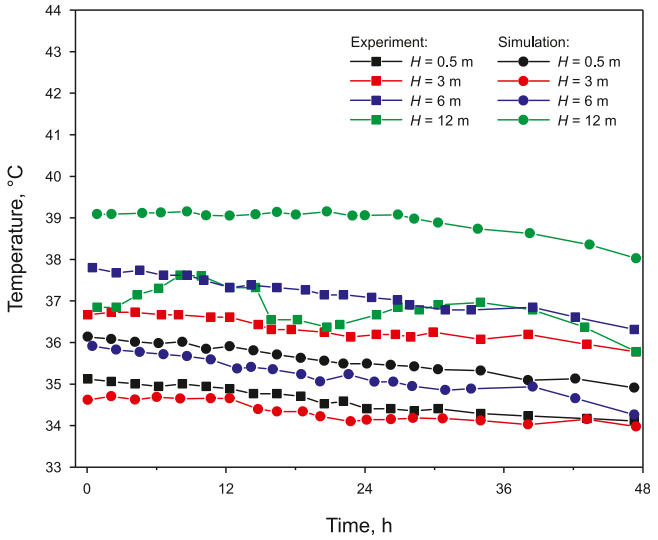

Fig. 11. Temperature change at different heights in the center of storage tank.

coupling characteristics between heat transfer and flow, with the impact flow generated by the agitator carrying away released heat from the heating tube and transferring it over a wider range. Moreover, two vortices form on both side of the impact flow, exhibiting a lower temperature within them. According to fluid mechanics principles, crude oil experiences uneven effect of stirring and heating during its flow. Simultaneously, it is influenced by viscosity, velocity and flow direction of crude oil become non-uniform, leading to vortex formation in certain regions. Consequently, heat exchange at these vortices occurs infrequently resulting in lower temperature within them as well. With an increase in τ, the proportion of high-speed crude oil in the direction of agitator gradually increases while vortex size gradually diminishes along with a decrease in low temperature regions proportionality. Additionally, mechanical stirring significantly affects temperature distribution at the lower boundary throughout computational domain and is the most significant in whole computational domain. The high temperature region essentially coincides with trajectory of impact flow which becomes more apparent as τ increases.

Fig. 15(a) and (b) shows that increasing in τ can increase the average velocity and fluidity of the crude oil, which in turn increases the average crude oil temperature. The increase in τ enhances stirring effect and increases the average velocity in the computational domain. As τ increases, the average velocity after

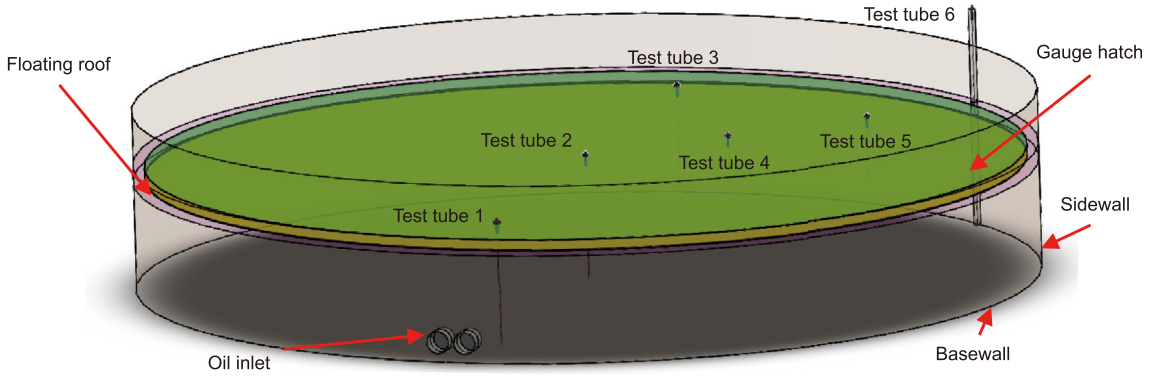

Fig. 10. Lay out of test tubes and the floating roof tank.

Table 4
Conditions of simulation for different cases.

Case	deflection angle θ, °	Stirring diameter D, mm	Stirring rate τ, rpm	Heating temperature T_{heat}, °C	Heating time, h	Ambient temperature, °C	Initial crude oil temperature, °C
1	0	500	350	80	2	−20	42
2	0	500	200				
3	0	500	500				
4	θ_1 7 (Horizontal)	500	350				
5	θ_1 12 (Horizontal)	500	350				
6	θ_2 7 (Vertical)	500	350				
7	θ_2 12 (Vertical)	500	350				
8	0	400	350				
9	0	600	350				

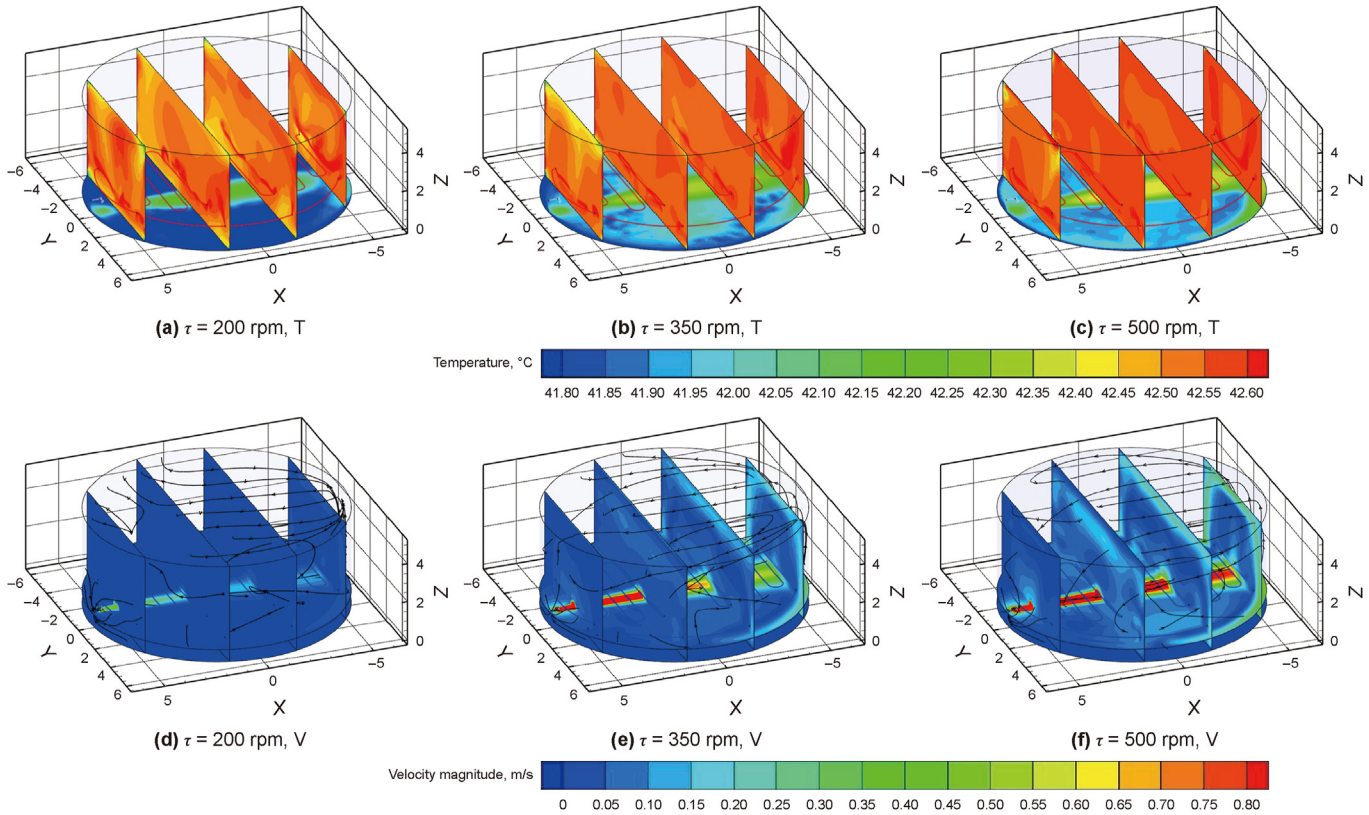

Fig. 12. Effect of stirring rate on three-dimensional temperature and velocity fields (t = 2 h).

stabilization are 0.038 m/s, 0.073 m/s and 0.107 m/s, respectively. After 2 h of stirring and heating, as τ increases, the average crude oil temperature increase to 42.568 °C, 42.586 °C and 42.600 °C, respectively, and the heating rates are 0.284 °C/h, 0.293 °C/h and 0.300 °C/h, respectively. The increase in τ significantly improves the fluidity of the crude oil in computational domain, enhances the heat transfer between the crude oil and increases the average temperature.

(2) Effect of stirring rate on key region in storage tank

Low temperature region has always been a key factor restricting the safe operation for crude oil storage tank, and too low temperature will lead to crude oil gel, which in turn will affect safe storage and scheduling in the tank (Zhang et al., 2012, 2020b). The location and coverage of low temperature region are of great significance to the safe operation and management for the storage tank, and the main function of mechanical stirring is to weaken the coverage of the low temperature region and increase its temperature. Accidents in the tank caused by low temperature mainly include capsizing of the floating roof on the topwall, condensation in storage tank caused by the blockage of loading and unloading operation, and floating roof descent influenced by the oil mountain formed at the basewall. Therefore, the temperature distribution of crude oil and low temperature regions in several boundaries are focused.

① Effect of stirring rate on topwall and basewall of storage tank

The temperature distribution in the upper boundary at different τ is illustrated in Fig. 16. Due to the limited influence of the agitator on the boundary junction and it away from the heating tube, and heat dissipation between this region and the low temperature environment, there is a low temperature around the upper boundary. For the inner region within the upper boundary, when τ is small, crude oil near this area experiences minimal stirring and exhibits slow flow with infrequent heat exchange, leading to lower temperature and a more uniform distribution within this inner region. As τ increases, stirring effects become more prominent. When τ increases to 350 rpm, a significant amount of heat is carried away by impact flow and accumulates in regions opposite the

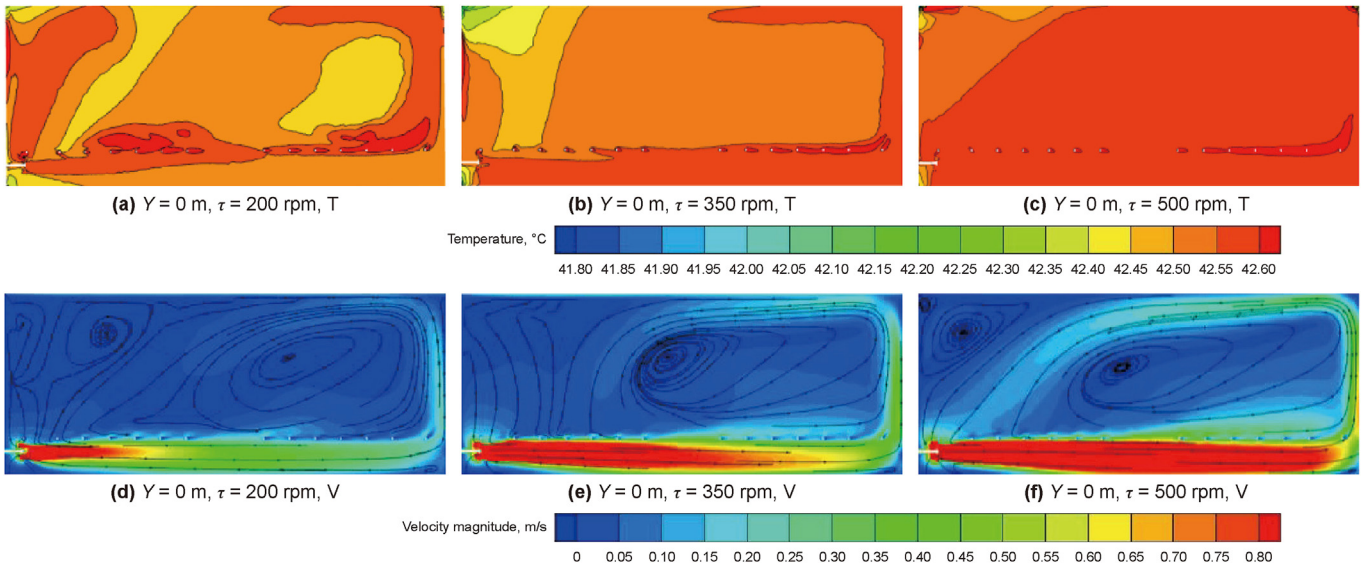

Fig. 13. Effect of stirring rate on temperature and velocity fields in $Y = 0$ m ($t = 2$ h).

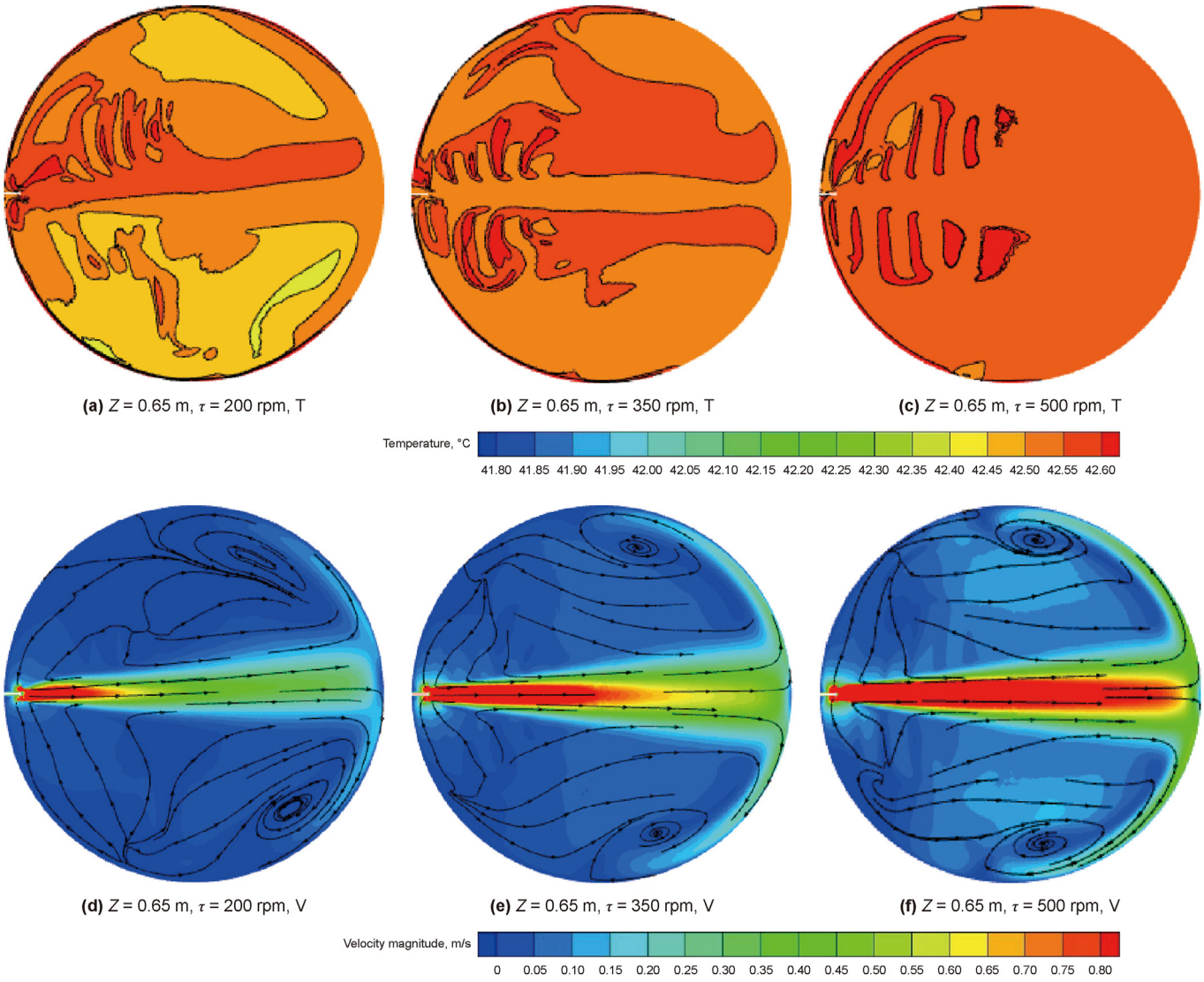

Fig. 14. Effect of stirring rate on temperature and velocity fields in $Z = 0.65$ m ($t = 2$ h).

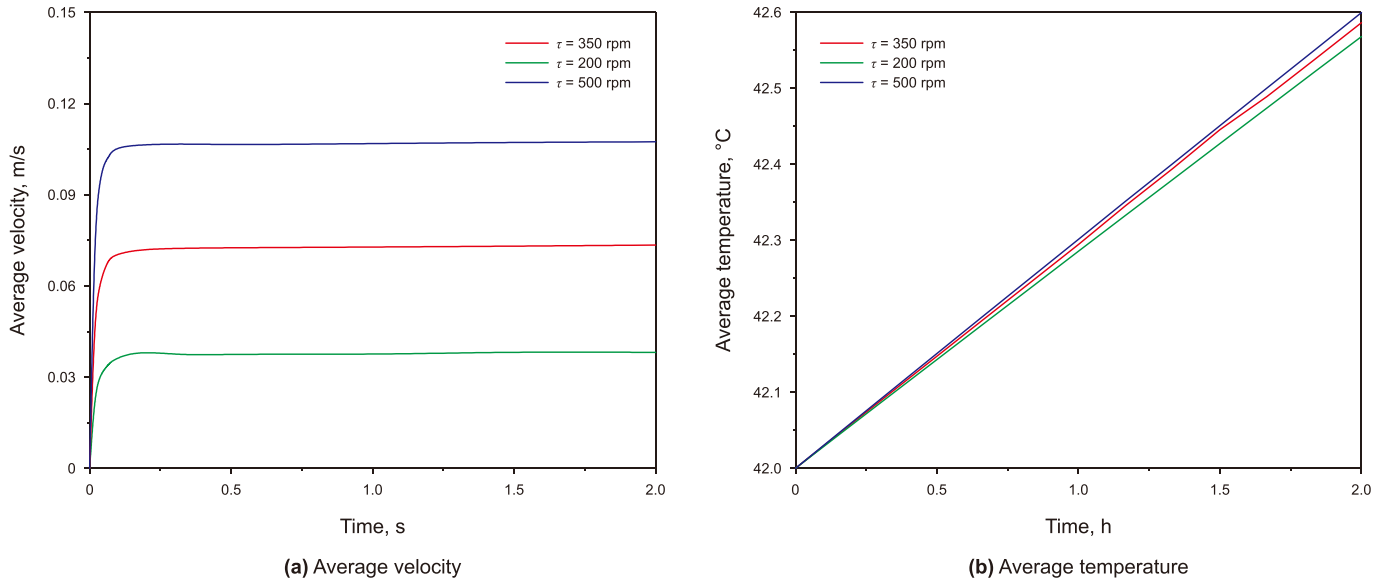

Fig. 15. Effect of stirring rate on average velocity and temperature.

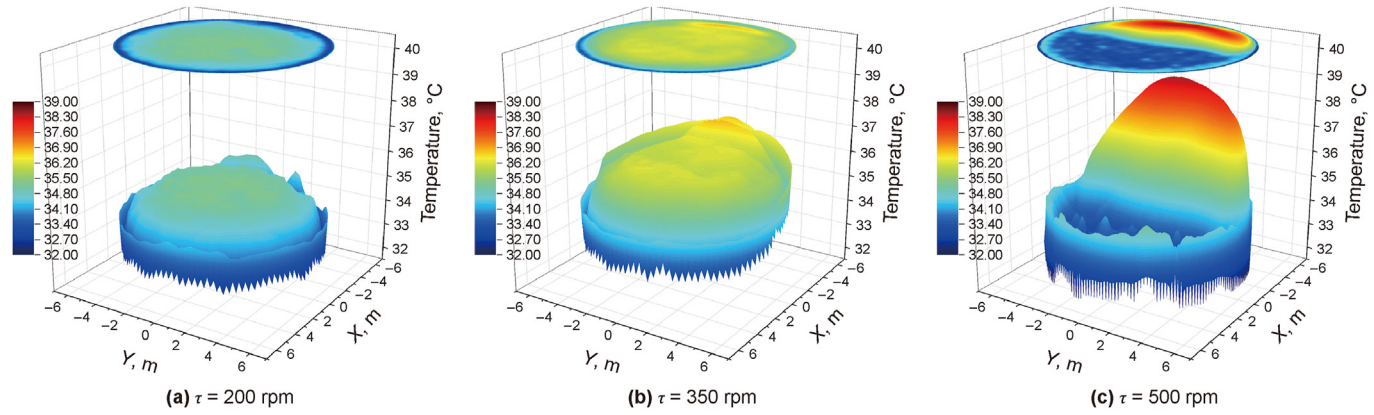

Fig. 16. Effect of stirring rate on temperature field in upper boundary ($t = 2$ h).

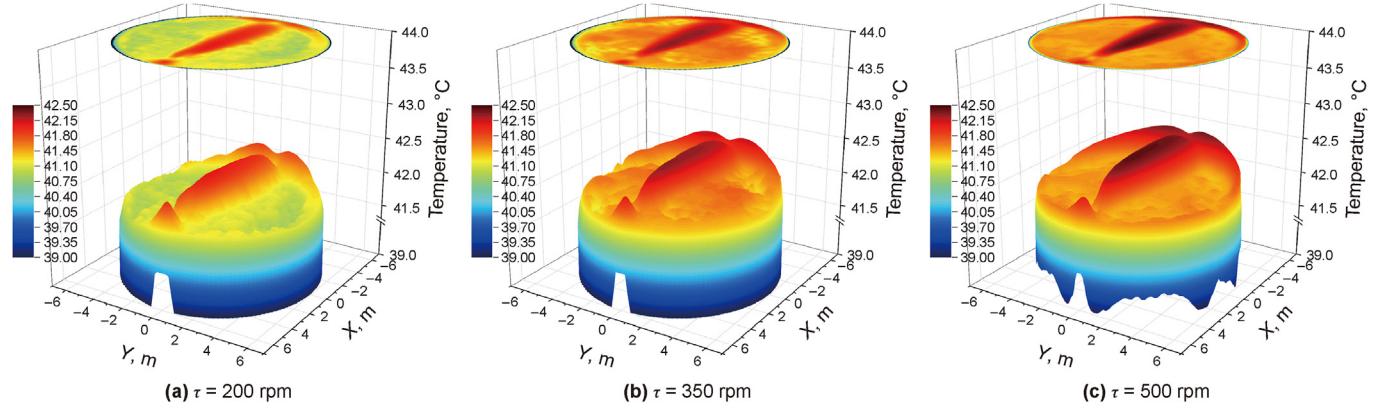

Fig. 17. Effect of stirring rate on temperature field in lower boundary ($t = 2$ h).

agitator. Consequently, temperature in these areas increase while those in regions located above the agitator decrease, causing a gradual decrease in temperature uniformity within the upper boundary. When τ reaches 500 rpm, even more heat accumulates in regions opposite to that of the agitator which further raises temperature there; meanwhile, temperature in regions above the agitator continue to decline resulting in decreased temperature uniformity throughout this entire upper boundary where both-

ends distribution pattern emerges. By combining these findings with velocity field distribution at $Y = 0$ m shown in Fig. 13, it can be observed that a small vortex above the upper boundary area is little affected by the central large vortex; fluidity within this small vortex location becomes poor with infrequent heat exchange occurring consequently leading to reduced temperature specifically for regions located above agitator. For topwall of the actual tank, the slow τ would lead to a low temperature in crude oil at the topwall of the tank, a layer of high-viscous crude oil at low temperature could adhere to the bottom of floating roof. It would affect normal floating for the floating roof When the liquid level in the tank changes, resulting in a blockage accident. When τ is quick, the distribution of crude oil temperature at the topwall of the tank is extremely uneven, which will also cause the floating roof capsizing. Reasonably increasing τ is of practical significance for improving the temperature and temperature uniformity of crude oil at the topwall and ensuring crude oil with great fluidity.

The temperature distribution in the lower boundary at different τ is illustrated in Fig. 17. Overall, the synergy of tubular heating and mechanical stirring results in higher temperature along the stirring direction and lower temperature on both sides of this direction. However, due to slight stirring effect and heat dissipation with the external low temperature environment, the temperature around the lower boundary remains relatively low. Mechanical stirring has a significant impact on heat transfer, leading to higher crude oil temperature along the stirring direction and an upward trend in center temperature as τ increases. Additionally, increased overall velocity causes more heat to return to the vicinity of the agitator after colliding with side boundaries, promoting flow and heat transfer of crude oil while increasing temperature around both sides of the stirring direction and at the lower boundary region. Consequently, there is a gradual improvement in overall temperature uniformity. For basewall of the actual tank, when τ is slow, the temperature on both sides of the stirring direction is low. Accompanied by the deposition of heavy component sludge, a low temperature region and gelled oil of uneven height would be formed at the basewall, and if the height of the gelled oil is too high, it could affect the normal delivering and receiving operation in the storage tank. With the increase of τ, the temperature and temperature uniformity of the crude oil near the basewall of the tank improve, but the heating effect from stirring and heating could decrease. In the upper and lower boundaries, the crude oil located on the opposite side of the agitator has a higher temperature and greater fluidity. If the oil-inlet and oil-outlet are located in this region, it will be conducive to the safe operation of delivering and receiving for crude oil. Proper installation positioning of the agitator and moderate τ are conducive to delivering and receiving operations for crude oil.

The heat dissipation through the upper and lower boundaries in different τ is illustrated in Fig. 18(a) and (b), respectively, with temperature fields being the main influencing factor. It can be observed that the heat dissipation in both boundaries exhibits more pronounced changes initially, but gradually stabilizes due to the stirring effect. With increasing τ, as shown in Figs. 16 and 17, the temperature in upper and lower boundaries rises, leading to an increase in heat dissipation at different τ. Specifically, the average growth rate for heat dissipation in the upper boundary is approximately 1%, while it is around 0.4% for the lower boundary. Simultaneously, as heating progresses, there is an overall rise in crude oil temperature along with an increased temperature difference between crude oil and its low temperature external environment; consequently resulting in enhanced heat dissipation.

② Effect of stirring rate on sidewall of storage tank

According to the simulation results, in comparison with the upper and lower boundaries of the computational domain, it is observed that the temperature of the side boundary is relatively lower. Consequently, this facilitates the adsorption and accumulation of gelled oil on the sidewall. Similarly, such deposition of gelled oil on the sidewall can lead to blockages in both delivery and receiving operations within storage tank, thereby impacting normal floating of floating roofs and potentially causing accidents. So, the region below 40 °C in the computational domain at different τ is defined as the low-temperature region and its distribution is shown in Fig. 19. It shows that with the increase of τ, the coverage of the low-temperature region decreases significantly from 69.49 m^3 to 12.48 m^3, and the average temperature of the low-temperature region increases from 35.49 °C to 37.24 °C. The presence of gelled oil in the boundary on the opposite side of the agitator is significantly reduced, thereby greatly improving the low-temperature region within the boundary. Proper installation positioning of the agitator and moderate τ could eliminate gelled oil near both the oil-inlet and oil-outlet, ensuring safe operation during crude oil

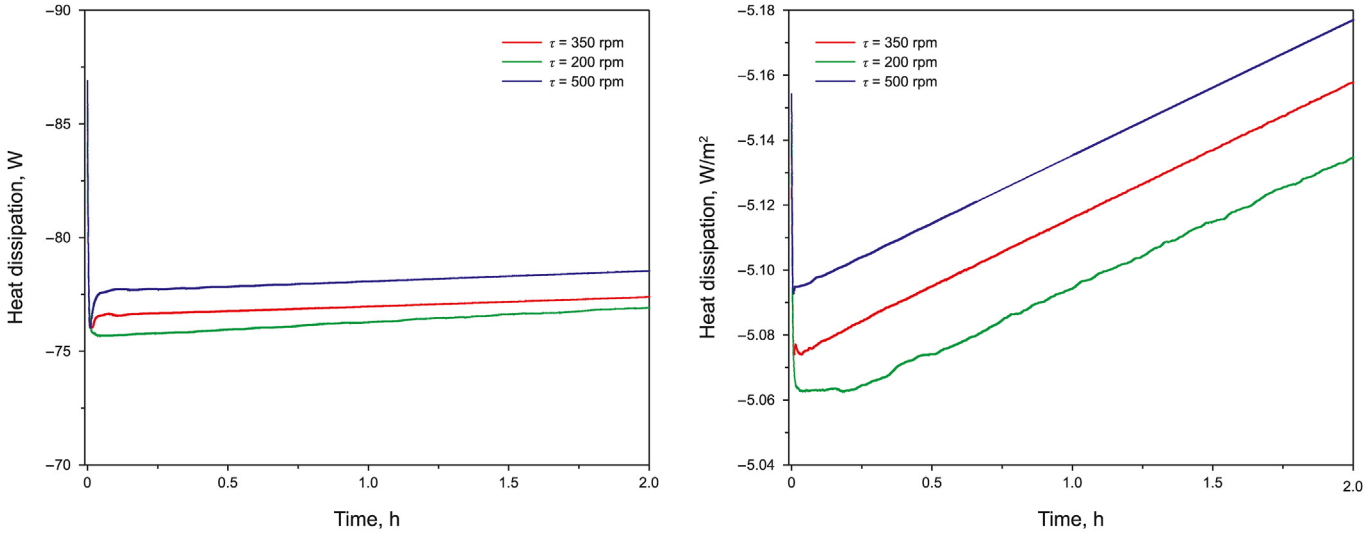

(a) Heat dissipation in upper boundary

(b) Heat dissipation in lower boundary

Fig. 18. Effect of stirring rate on heat dissipation through boundaries.

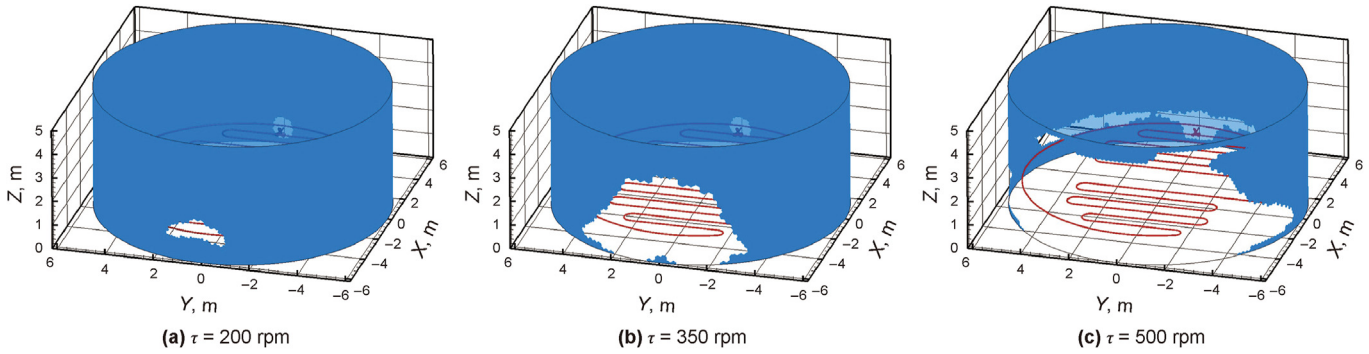

Fig. 19. Low-temperature region distribution at different stirring rate (t = 2 h).

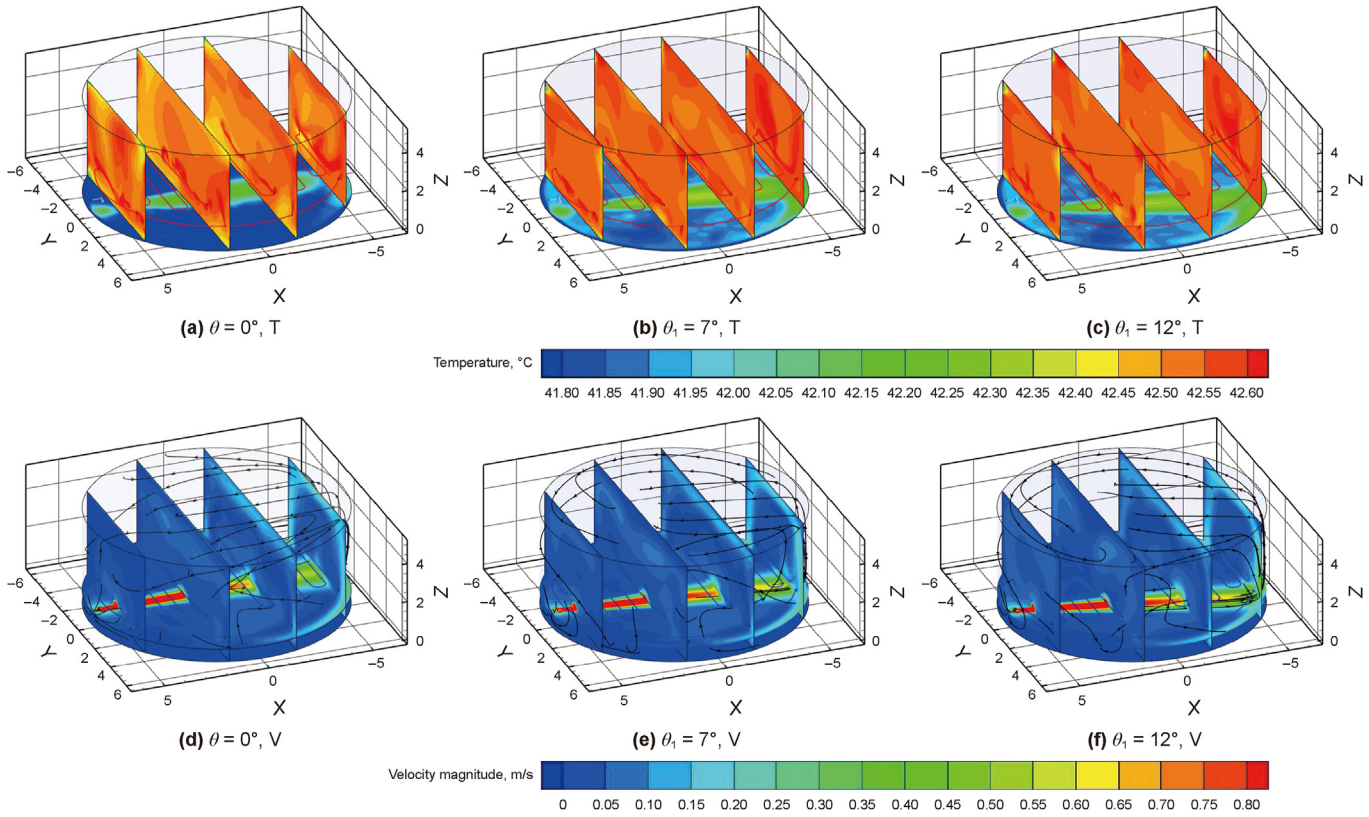

Fig. 20. Effect of horizontal deflection angle on three-dimensional temperature and velocity fields (t = 2 h).

delivery and receiving.

4.2.2. Horizontal deflection angle of agitator

(1) Effect of horizontal deflection angle on central region in storage tank

The temperature and velocity fields after 2 h of heating at different θ_1 are illustrated in Fig. 20. Comparing the temperature and velocity fields shown in Fig. 20, it can be observed that the overall velocity field remains relatively unchanged across varying θ_1. However, as θ_1 increases, both the strong impact flow generated by the agitator and the high temperature regions at the lower boundary deflect accordingly, so that the heat released from heating tube form different heat transfer paths under the effect of forced convection. Moreover, an increase in θ_1 enhances temperature uniformity above the agitator and near the top of storage tank. Conversely, stirring effect has minimal influence on low temperature regions at junctions between different boundaries, resulting in a decrease in temperature and subsequent expansion of coverage area. Nevertheless, due to consistent stirring strength, similar overall flow trends are observed under different θ_1 with only slight changes in the overall velocity field, thus causing insignificant changes in overall temperature distribution. Similarly for sections $X = -4.8$ m, -1.6 m, 1.6 m and 4.8 m, the average temperature remain consistently highest at $X = -4.8$ m and lowest at $X = 4.8$ m. As θ_1 increases, the temperature difference between $X = \pm 4.8$ m decreases from 0.03 °C to 0.02 °C. This effect of θ_1 on the temperature in each section is evident from the contours shown in Fig. 21.

The formation of a large vortex in the central region can be observed from Fig. 21 when high temperature crude oil flows near the heating tube under the influence of θ_1. This vortex is generated by the impact of the agitator, resulting in higher fluidity and more

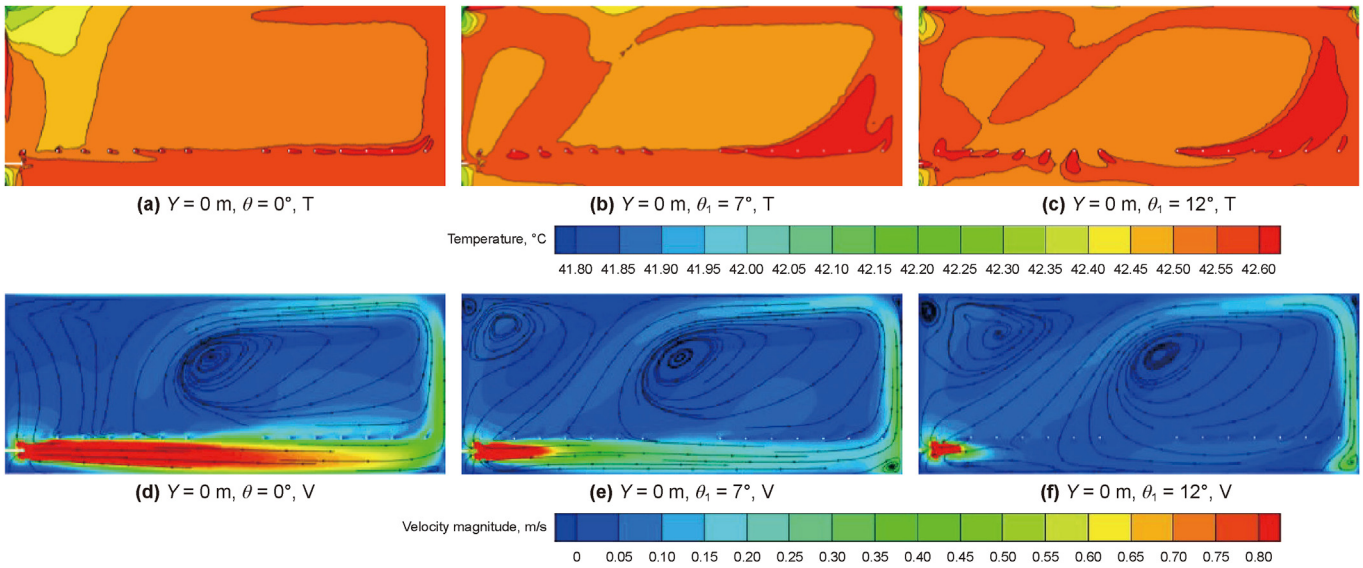

Fig. 21. Effect of horizontal deflection angle on temperature and velocity fields in $Y = 0$ m ($t = 2$ h).

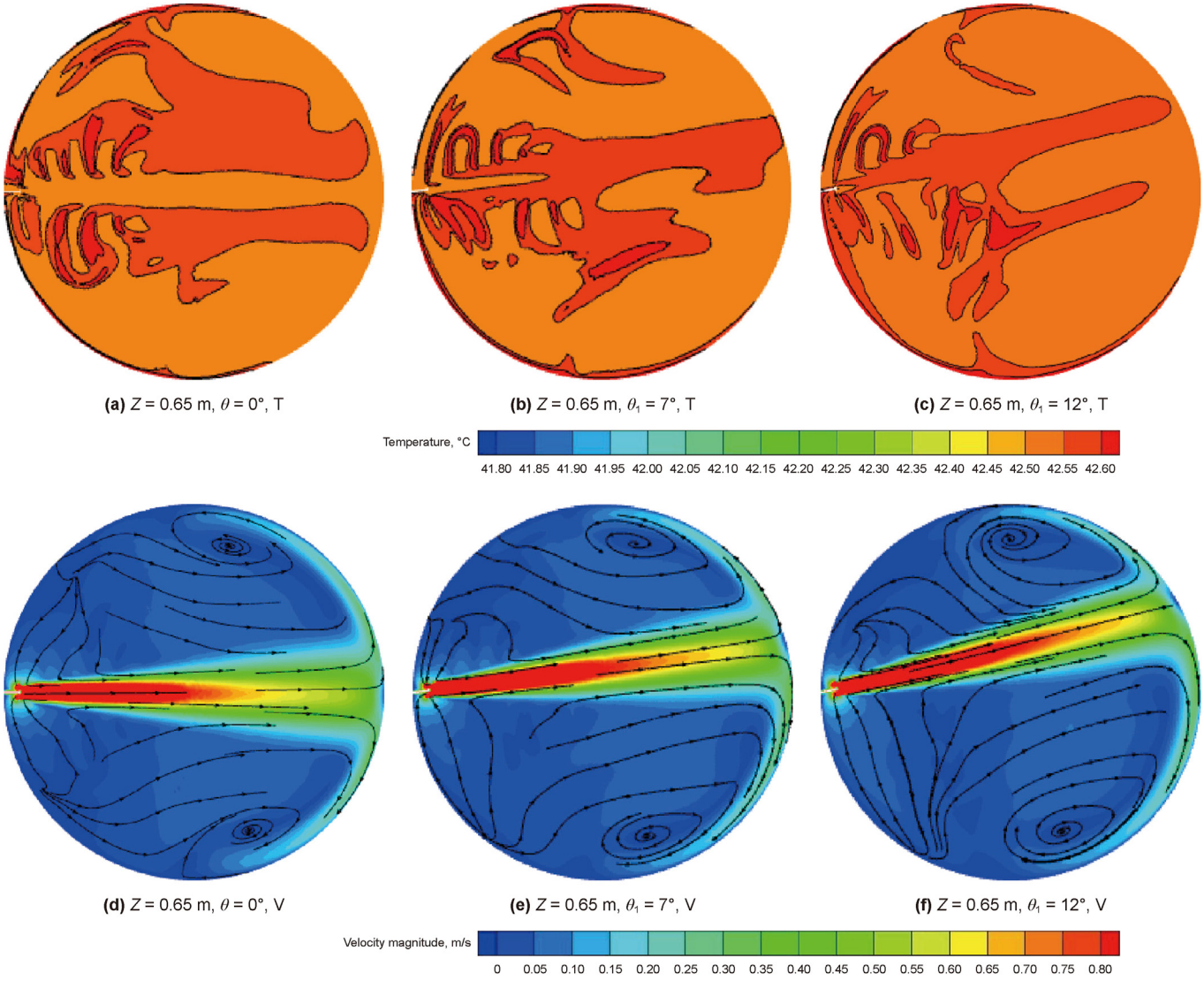

Fig. 22. Effect of horizontal deflection angle on temperature and velocity fields in $Z = 0.65$ m ($t = 2$ h).

intense heat transfer within the vortex-covered region, leading to elevated temperature compared to other areas. Conversely, regions unaffected by this vortex experience lower temperature and are more prone to forming low temperature region. By comparing the temperature field at $Y = 0$ m in Fig. 21(a)–(c), it becomes evident that an increase in θ_1 leads to a greater proportion of high temperature crude oil at $Y = 0$ m and significantly improves the low temperature region above the agitator. To further illustrate the temperature field variation at $Y = 0$ m, Fig. 21(d)–(f) presents the results. As θ_1 increases, the high-speed crude oil directly in front of the agitator at $Y = 0$ m is also deflected, a larger θ_1 leads a smaller proportion of high-speed crude oil at the bottom. The flow direction of crude oil near the heater on the side of the agitator gradually deflects downwards with increasing θ_1, while the flow direction of crude oil near and far from the agitator deflects upwards, resulting in variations in high temperature crude oil distribution near heating tubes. Meanwhile, as θ_1 increases, the vortex in the center gradually moves away from the agitator and a smaller vortex forms above it. This new vortex enhances the fluidity of crude oil in the region above the agitator and reduces uneven temperature distribution, although complete elimination is not achieved. Due to the wide influence range of the vortex at the center which does not change obviously with time, the temperature in center of $Y = 0$ m does not change much either. Consequently, the temperature and velocity distribution in the vicinity of the lower boundary and its surrounding region are provided. As shown in Fig. 22(a)–(f), $Z = 0.65$ m represents the plane where the agitator is located, where there exists a pronounced interaction between flow dynamics and heat transfer. At $Z = 0.65$ m, the crude oil exhibits an increased velocity in the direction of agitator, resulting in the formation of two vortices on both sides centered around the impact flow after colliding and rebounding with the opposing wall. The distribution of vortices is deflected with the increase of θ_1, and the temperature at the vortices is lower. Furthermore, the presence of the agitator significantly affects the temperature distribution at the lower boundary, coinciding with the trajectory of impact flow where high temperature regions are predominantly observed.

Fig. 23(a) and (b) shows that change in θ_1 has no significant effect on the average velocity and average crude oil temperature. The change of θ_1 for the agitator does not affect the intensity of stirring effect, only changes the direction of stirring effect, and the flow field is also deflected accordingly, but its overall trend is basically constant. With the increase of θ_1, the average velocity after stabilization are 0.073 m/s, 0.072 m/s and 0.075 m/s, respectively, and the overall velocity field do not change significantly. After 2 h of stirring and heating, the average crude oil temperature are 42.586 °C, 42.586 °C and 42.585 °C, respectively, and the maximum temperature difference is within 0.001 °C. The change in θ_1 for the agitator has no significant effect on temperature and velocity fields.

(2) Effect of horizontal deflection angle on key region in storage tank

① Effect of horizontal deflection angle on topwall and basewall of storage tank

The temperature distribution in the upper boundary at different θ_1 is illustrated in Fig. 24. Overall, as θ_1 increases, the temperature around the upper boundary remains low and relatively stable, while significant changes occur in the inner region of the upper boundary. When θ_1 is 0°, it can be observed that the flow of crude oil near the upper boundary is influenced by the central vortex generated from the agitator. Heat is transferred from regions away from the agitator towards regions close to it, resulting in a gradual decrease in temperature. With increasing θ_1, a small vortex forms above the agitator near the upper boundary which is minimally affected by the central large vortex. Heat transfer within this small vortex primarily relies on natural convection and occurs infrequently; thus, heat dissipates to external low temperature surroundings leading to lower temperature near the agitator region compared to cases without deflection, exhibiting a both-ends distribution. Consequently, overall temperature uniformity decreases within the upper boundary due to varying θ_1. The θ_1 significantly influences both temperature and uniformity of crude oil within this region. For topwall of the actual tank, increasing θ_1 will lead to the reduction of the crude oil temperature and the uneven temperature distribution in the topwall of the tank, the formation of a local low temperature area and accelerate the formation of gelled oil. When the liquid level in the tank changes, it would affect the floating roof normal floating, and even cause the floating roof capsizing, affecting the normal production.

The temperature distribution in the lower boundary at different θ_1 is illustrated in Fig. 25. Overall, the synergy of heating and

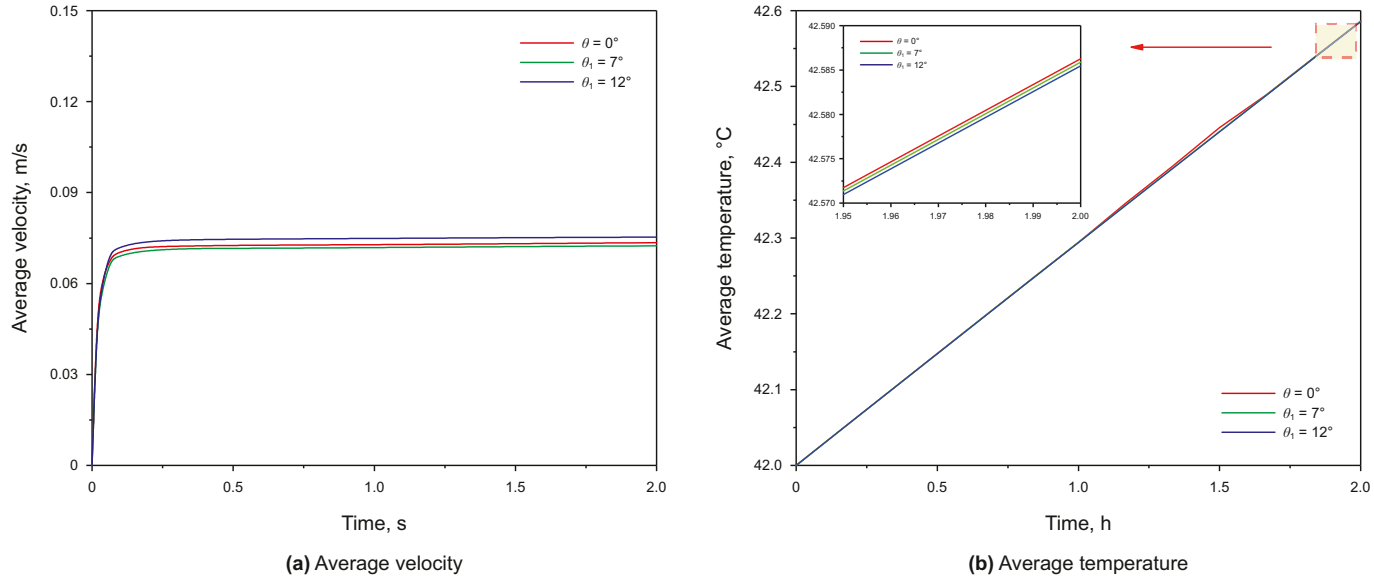

(a) Average velocity **(b)** Average temperature

Fig. 23. Effect of horizontal deflection angle on average velocity and temperature.

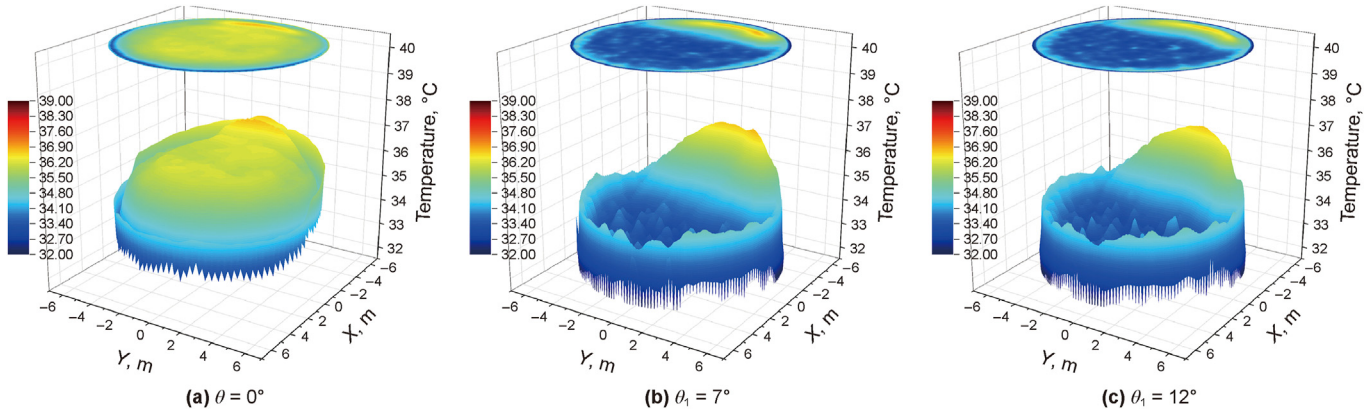

Fig. 24. Effect of horizontal deflection angle on temperature field in upper boundary ($t = 2$ h).

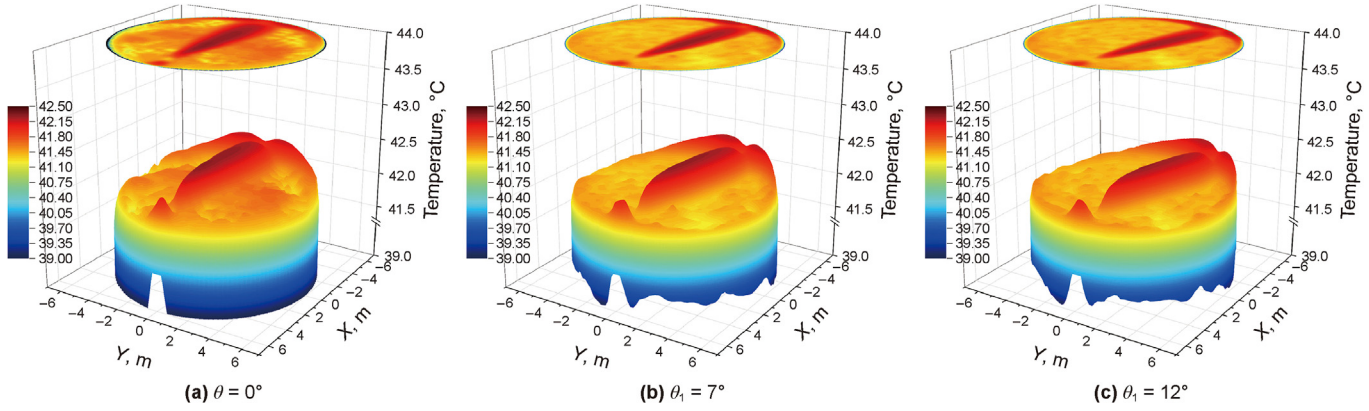

Fig. 25. Effect of horizontal deflection angle on temperature field in lower boundary ($t = 2$ h).

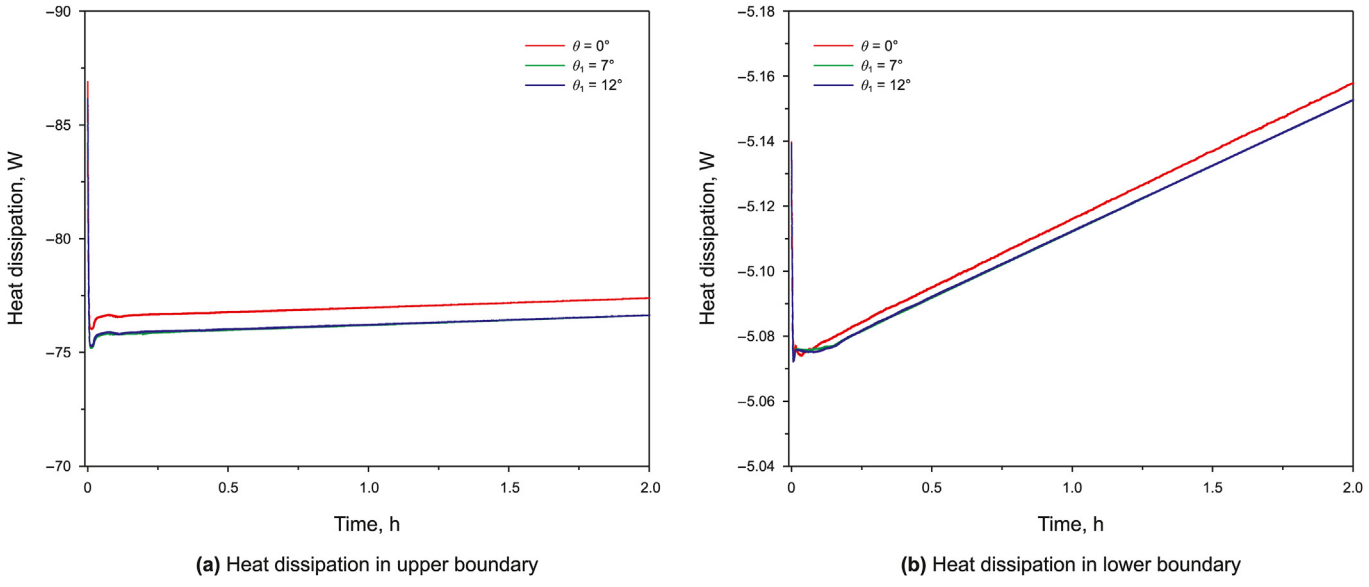

Fig. 26. Effect of horizontal deflection angle on heat dissipation through boundaries.

stirring results in higher temperature along the stirring direction, while temperature on both sides of this direction and around the lower boundary remains very low. As θ_1 increases, there is a deflection observed in the position of high temperature crude oil in the center of the lower boundary. After colliding with the side boundary, high temperature crude oil flows along it, leading to a slight improvement in low temperature distribution around this boundary. With an increase in θ_1, there is an increased deflection

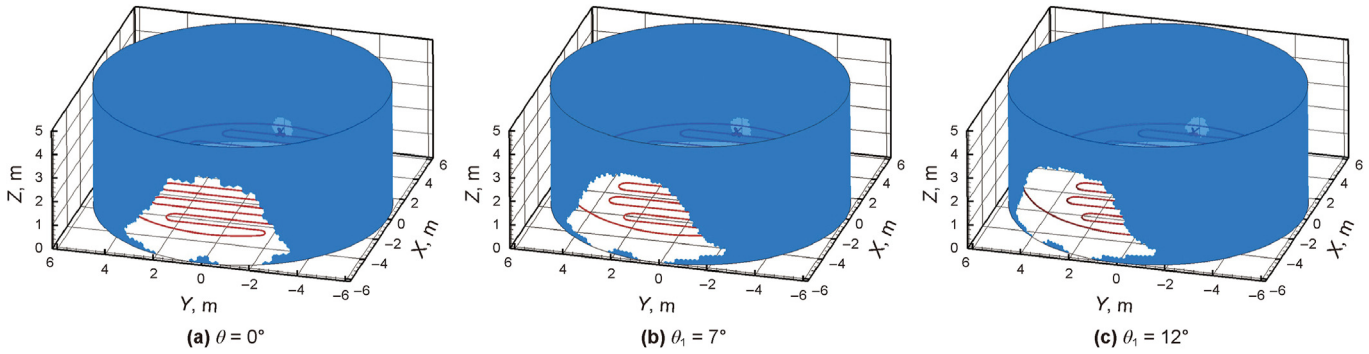

Fig. 27. Low-temperature region distribution at different horizontal deflection angle ($t = 2$ h).

angle for high temperature crude oil distributed along the agitator direction and a slight decrease in temperature on both sides of this direction. Consequently, there is an overall decrease in temperature within the lower boundary; however, temperature uniformity remains relatively unchanged. For basewall of the actual tank, θ_1 has no obvious effect on the temperature uniformity in the basewall, but it will decrease the overall temperature and accelerate the generation of gelled oil in the basewall, which could affect the normal delivering and receiving operations for crude oil. Increasing θ_1 could have an adverse effect on the temperature field for the upper and lower boundaries, which is not beneficial for the delivering and receiving operations. In the upper and lower boundaries, the crude oil located on the opposite side of the agitator has a higher temperature and greater fluidity. Proper installation positioning of the agitator is of practical significance for normal operation of the tank.

The heat dissipation in the upper and lower boundaries under different θ_1 is illustrated in Fig. 26(a) and (b), respectively. When combined with Figs. 24 and 25, it can be observed that as θ_1 increases, there is a decrease in overall temperature rise and heat dissipation at both the upper and lower boundaries. Compared with the case of 0°, when θ_1 is 7°, the heat dissipation decreases by 0.76 W/m^2 and 0.005 W/m^2 for the upper and lower boundaries, respectively. However, when θ_1 increases from 7° to 12°, the heat dissipation remains relatively stable at both boundaries. Furthermore, it should be noted that the temporal variation of heat dissipation follows a similar pattern as shown in Fig. 18.

② Effect of horizontal deflection angle on sidewall of storage tank

It can be seen from Fig. 27 that with the increase of θ_1, the coverage of low-temperature region is also deflected, but the overall proportion of low-temperature region does not change

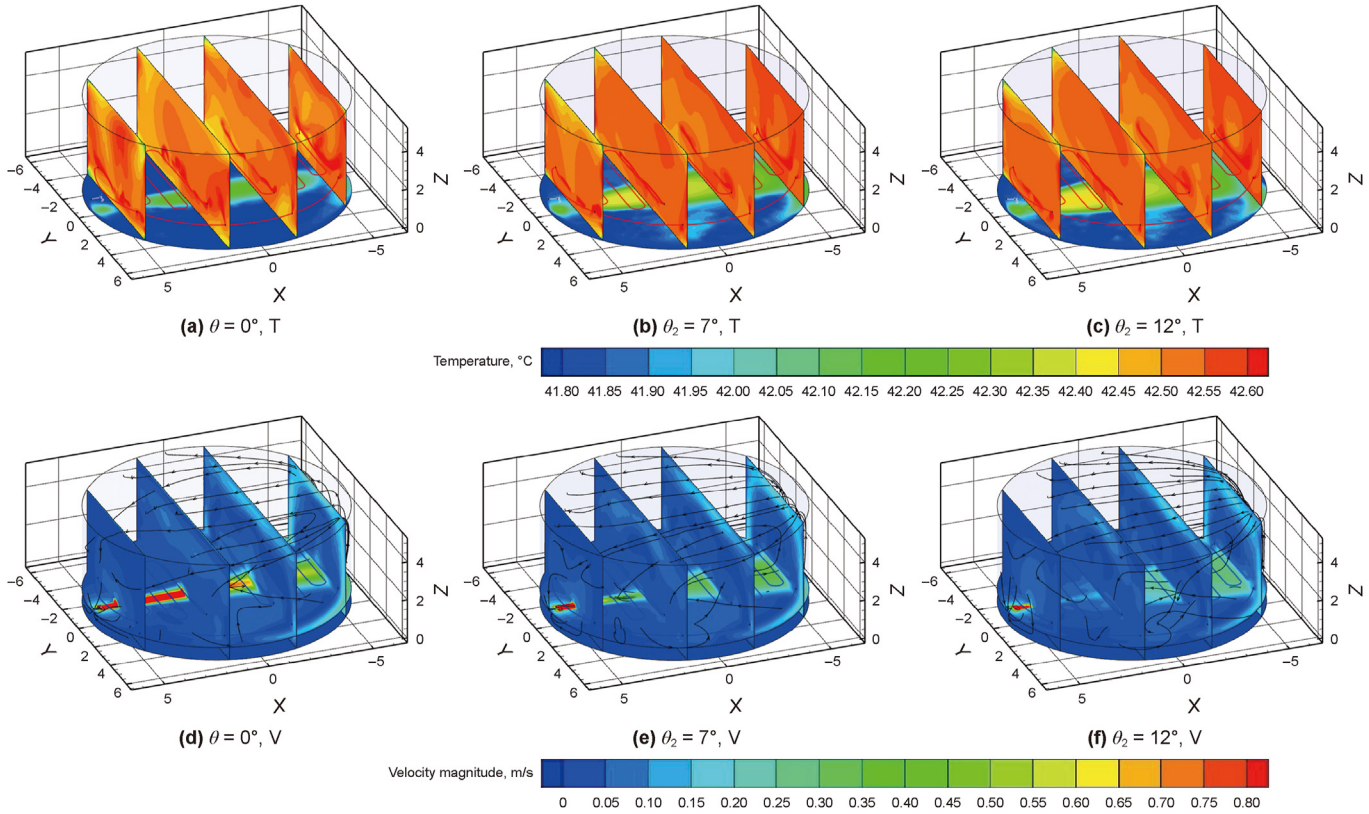

Fig. 28. Effect of vertical deflection angle on three-dimensional temperature and velocity fields ($t = 2$ h).

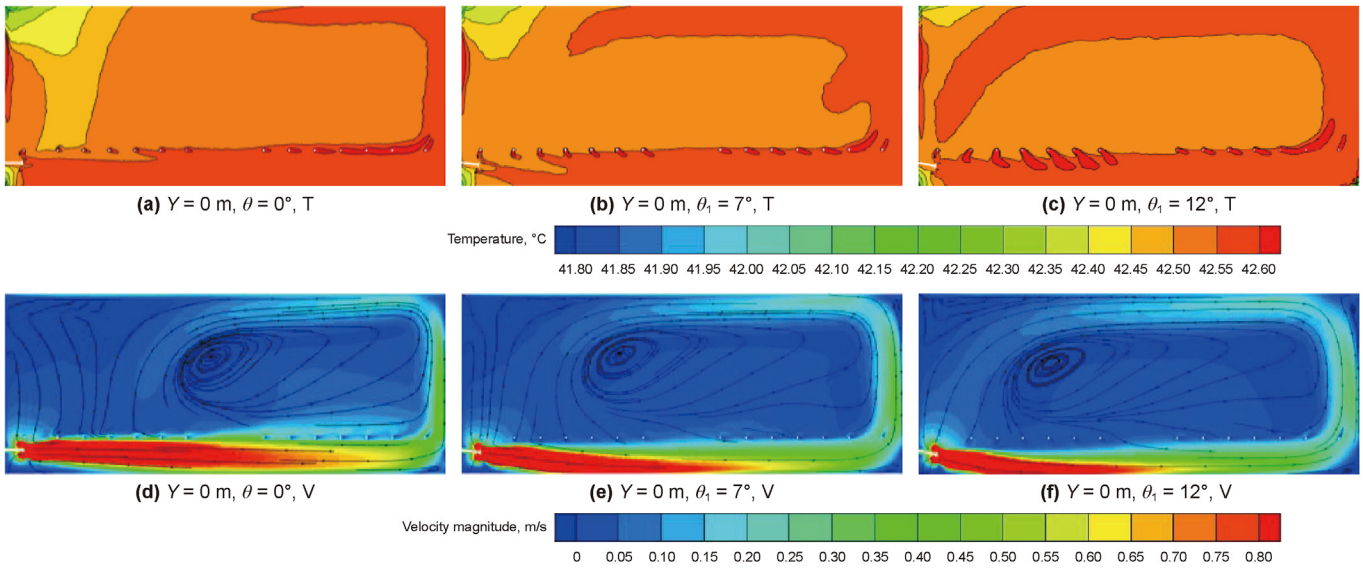

Fig. 29. Effect of vertical deflection angle on temperature and velocity fields in $Y = 0$ m ($t = 2$ h).

significantly. The volume of low-temperature region are 32.36 m^3, 31.91 m^3 and 31.71 m^3, and the average temperature of the region are 36.43 °C, 36.72 °C and 36.71 °C, respectively. The θ_1 only has an effect on the distribution in the low-temperature region. The oil-inlet and oil-outlet positions should always be located within the elimination range for gelled oil on the opposite side of the agitator.

4.2.3. Vertical deflection angle of agitator

(1) Effect of vertical deflection angle on central region in storage tank

The temperature and velocity fields after 2 h of heating at different θ_2 are illustrated in Fig. 28. Apart from the lower boundary, the overall velocity field remains relatively unchanged. As θ_2 increases, the proportion of high-speed crude oil in the direction of agitator decreases, while the proportion of high temperature region in the central direction of agitator at the lower boundary increases and is accompanied by a formation of lower temperature regions on both sides. However, due to the constant strength of stirring effect and similar overall flow trends under different θ_2, there is only slight variation observed in the overall velocity field with no significant changes in the overall temperature field. For sections $X = -4.8$ m, -1.6 m, 1.6 m and 4.8 m, $X = -4.8$ m consistently exhibits the highest average temperature while $X = 4.8$ m consistently shows the lowest average temperature throughout all θ_2. With increasing θ_2, there is a negligible change observed in temperature differences between $X = \pm 4.8$ m sections, which are 0.031 °C, 0.032 °C and 0.030 °C, respectively. The impact of θ_2 on temperature within each section can be seen in Fig. 29.

The influence of θ_2 can be observed in Fig. 29, where a prominent vortex is still formed in the central region. The fluidity of crude oil is higher near the vortex, resulting in more intense heat transfer and higher temperature compared to other regions. This phenomenon explains the presence of low temperature areas at the boundary. By comparing the temperature fields shown in Fig. 29(a)–(c), it becomes evident that increasing θ_2 leads to a reduction in the extent of low temperature crude oil above the agitator. To further illustrate the temperature field variation at $Y = 0$ m, as shown in Fig. 29(d)–(f), an increase in θ_2 leads to deflection and collision of high-speed crude oil towards the lower boundary by the agitator, resulting in a change in flow direction after rebound and subsequent loss of momentum, leading to a deceleration in velocity. Conversely, at the opposite boundary of the agitator and upper boundary, there is an increase in proportion of high-speed crude oil, which causes the vortex at center gradual close to agitator. The presence of this vortex enhances fluidity within its vicinity and facilitates heat exchange between crude oil, consequently elevating temperature and promoting uniformity within the low temperature region above the agitator. The distribution of the overall velocity field remains relatively unchanged, which leads to the minimal variations in temperature at the center of $Y = 0$ m. Conversely, the stirring effect significantly impacts the lower boundary and its surrounding region, leading to notable alterations in both temperature and velocity distribution. As shown in Fig. 30(a)–(f), $Z = 0.65$ m is the section where the agitator is located, the coupling characteristics of heat transfer and flow are also significant. At $Z = 0.65$ m, an increase in θ_2 results in a deflection of the high-speed crude oil driven by the stirring effect. Moreover, a larger θ_2 leads to a smaller proportion of high-speed crude oil and expands the range of influence for the agitator on the side boundary. The crude oil flows along the boundary after colliding with the boundary, forming vortices on both sides of the impact flow. As θ_2 increases, the position of the vortices moves along the side boundary to the opposite boundary of agitator, and the temperature at vortices is low. The presence of the agitator significantly influences the temperature distribution at the lower boundary, with a high temperature region that essentially aligns with the trajectory of impact flow.

Fig. 31(a) and (b) shows that the change in θ_2 also has no significant effect on the average velocity and temperature. The change of θ_2 only affects the direction of stirring effect, and the overall flow field trend is also basically consistent. With the increase of θ_2, the average velocity after stabilization are 0.073 m/s, 0.072 m/s and 0.070 m/s, respectively. After 2 h of stirring and heating, the average crude oil temperature are 42.586 °C, 42.581 °C and 42.580 °C, respectively, and the maximum temperature difference is only 0.006 °C. The change of θ_2 for agitator also has no significant effect on the temperature and velocity fields.

(2) Effect of vertical deflection angle on key region in storage tank

① Effect of vertical deflection angle on topwall and basewall of storage tank

The temperature distribution in the upper boundary at different

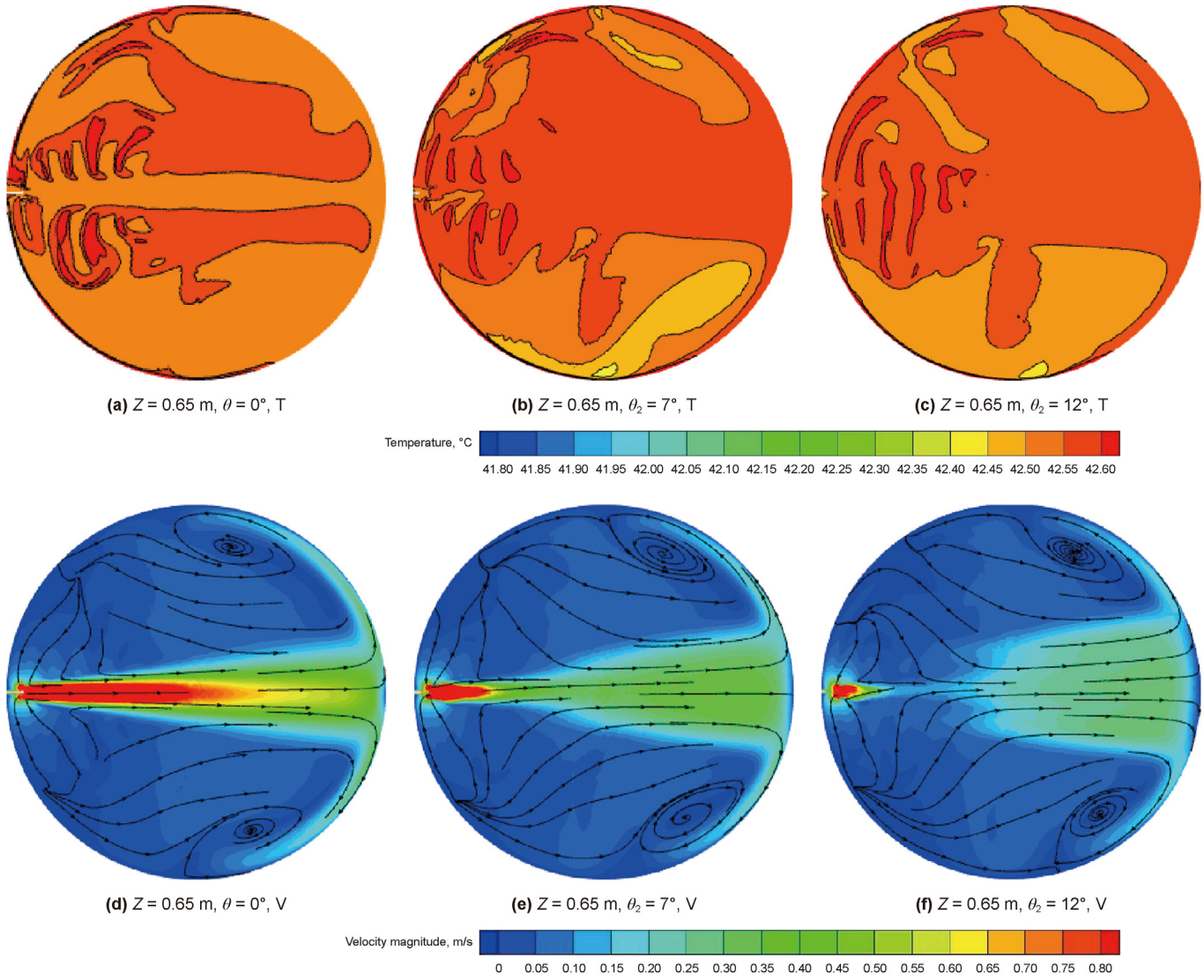

Fig. 30. Effect of vertical deflection angle on temperature and velocity fields in $Z = 0.65$ m ($t = 2$ h).

θ_2 is illustrated in Fig. 32. Overall, the temperature surrounding the upper boundary remains relatively low and exhibits minimal variation. However, significant changes in temperature occur within the inner region of the upper boundary, which leads to a gradual decrease in overall temperature. As θ_2 increases, high temperature crude oil deflects and collides with the lower boundary along the stirring direction, resulting in a reduction of momentum for high temperature crude oil after collision. Consequently, more heat is dispersed at the lower boundary, causing a relative decrease in the proportion of high temperature crude oil located within the upper boundary. For different θ_2, heat transfer occurs from regions distant from agitator towards regions close to agitator while gradually decreasing temperature. With the increase of θ_2, the proportion of the high temperature region on the opposite of the agitator in upper boundary decreases, the temperature around the upper boundary decreases, the overall temperature decreases accordingly and the temperature uniformity also decreases gradually.

The temperature distribution in the lower boundary at different θ_2 is illustrated in Fig. 33. Overall, higher temperature are observed along the stirring direction, while lower temperature are found in the regions on both sides of the stirring direction and around the lower boundary. As θ_2 increases, the high temperature crude oil along the stirring direction deflects and collides with the lower boundary, resulting in a decrease in momentum after collision and increased heat dispersion at the lower boundary. Subsequently, crude oil with reduced momentum continues to flow along the side boundary after colliding with the boundary. This process leads to an increase in temperature along the stirring direction and a decrease in temperature within regions located on both sides of it. With further increase of θ_2, there is a gradual rise in crude oil temperature along the stirring direction accompanied by an increasing proportion of high temperature crude oil; meanwhile, temperature on both sides of the stirring direction gradually decrease. Consequently, overall temperature uniformity decreases. For basewall of the actual tank, θ_2 has the same effect on crude oil at topwall and basewall of the tank as θ_1, large deflection angles have an adverse effect on the normal operation of crude oil storage tank.

The heat dissipation in the upper and lower boundaries under different θ_2 is illustrated in Fig. 34(a) and (b), respectively. When compared with Figs. 32 and 33, it can be observed that an increase in θ_2 leads to a rise in overall temperature while causing a decrease

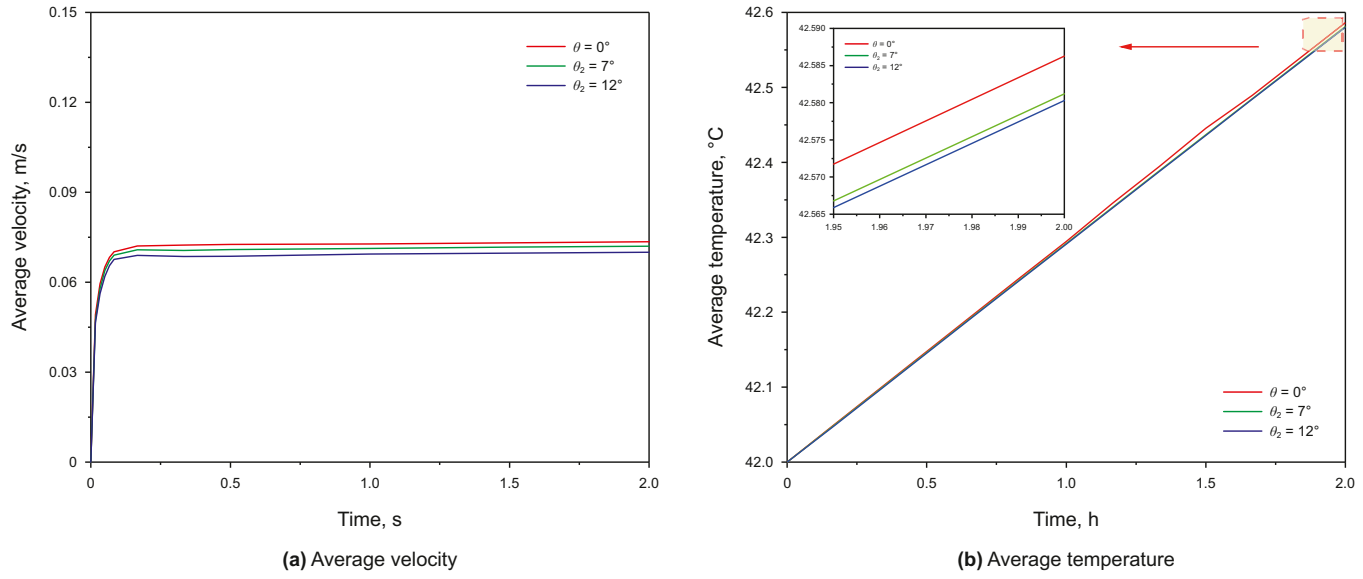

Fig. 31. Effect of vertical deflection angle on average velocity and temperature.

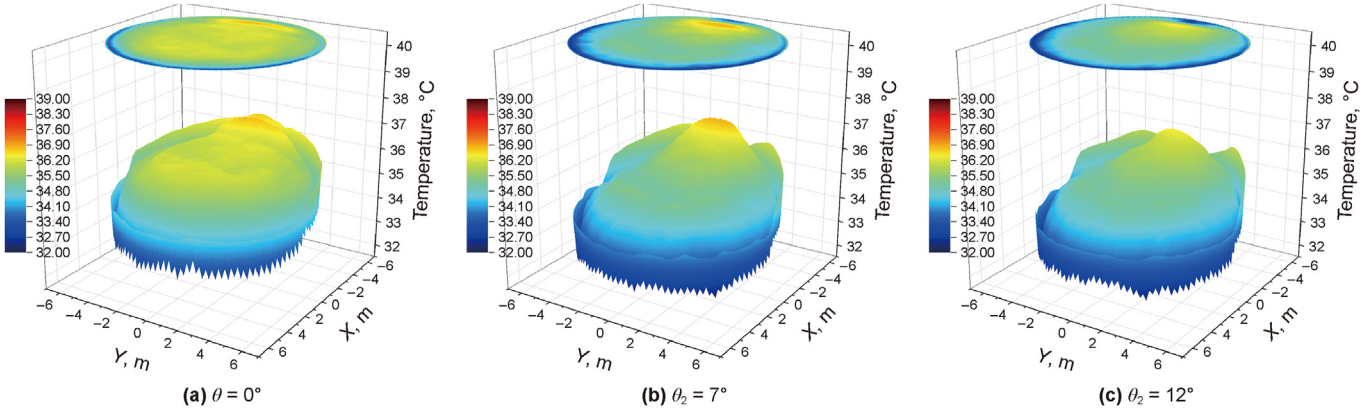

Fig. 32. Effect of vertical deflection angle on temperature field in upper boundary (t = 2 h).

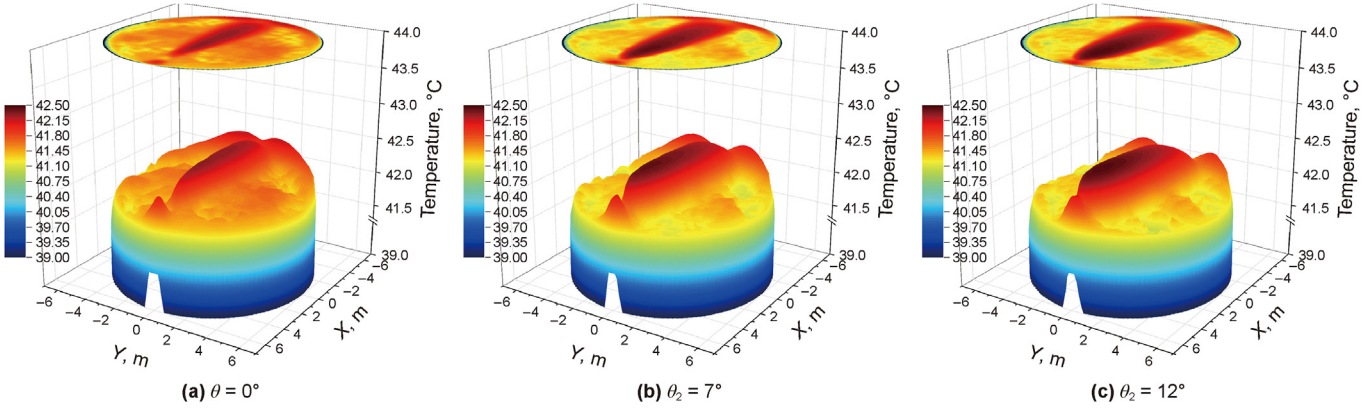

Fig. 33. Effect of vertical deflection angle on temperature field in lower boundary (t = 2 h).

in heat dissipation at both the upper and lower boundaries. Specifically, when the deflection angle is increased from 0° to 7°, the heat dissipation decreases by 1.5 W/m^2 and 0.007 W/m^2 for the upper and lower boundaries, respectively. However, as θ_2 increases from 7° to 12°, there is no significant change in heat dissipation at either boundary. Furthermore, the temporal variation of heat dissipation follows a similar pattern as shown in Fig. 18.

② Effect of vertical deflection angle on sidewall of storage tank

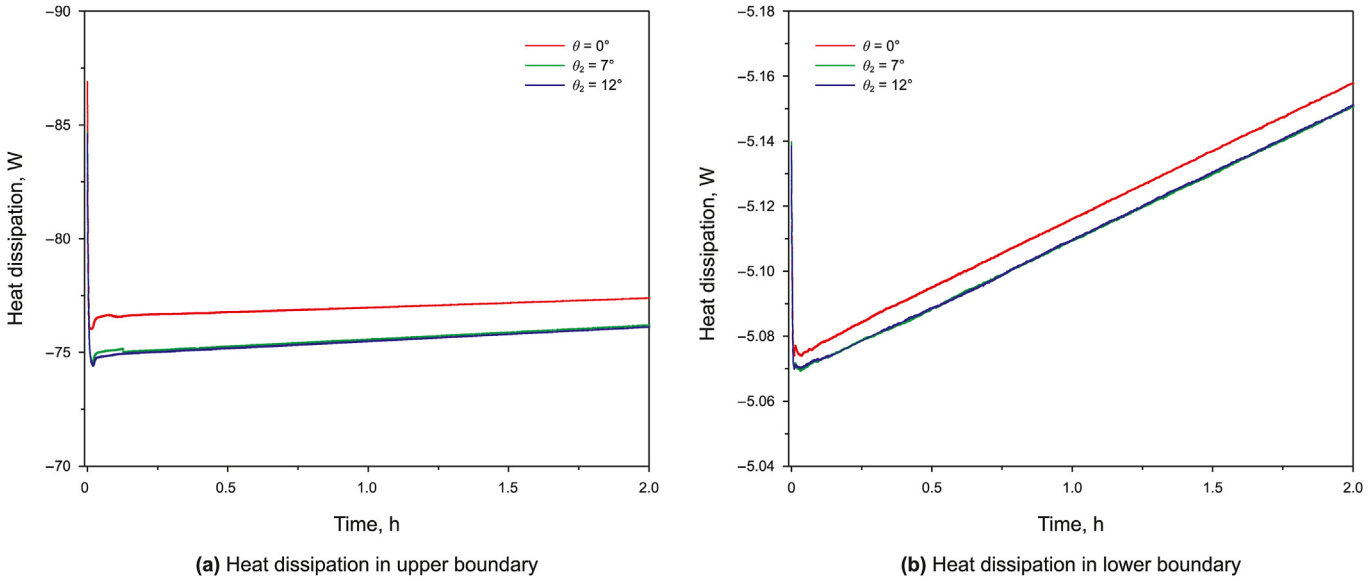

Fig. 34. Effect of vertical deflection angle on heat dissipation through boundaries.

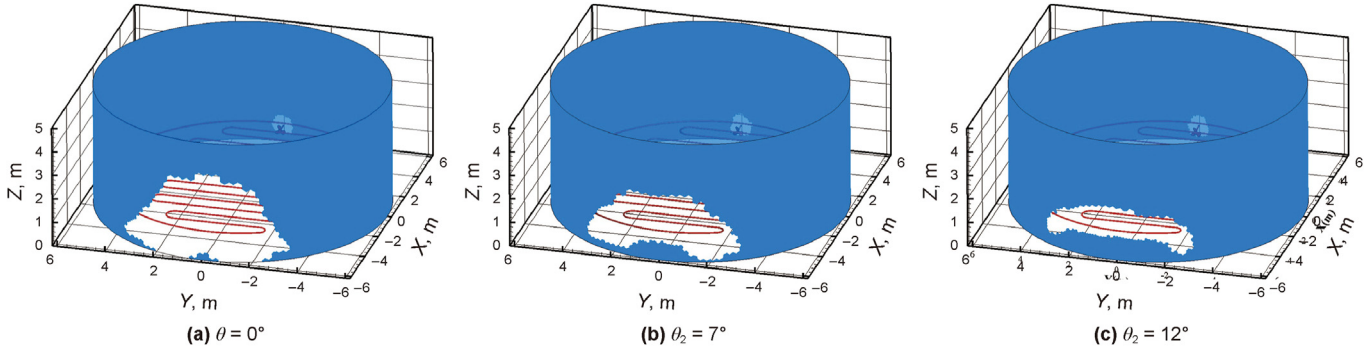

Fig. 35. Low-temperature region distribution at different vertical deflection angle (t = 2 h).

It can be seen from Fig. 35 that with the increase of θ_2, the volume of the low-temperature region are 32.36 m^3, 32.70 m^3 and 33.25 m^3, and the average temperature of it are 36.43 °C, 36.09 °C and 35.97 °C, respectively. The volume and average temperature in the low-temperature region remained unchanged, while there is an increase in the coverage of gelled oil on the opposite side of the agitator. This increase in θ_2 can impact both crude oil delivery and receiving operations, potentially leading to blockages at the oil-inlet and oil-outlet.

4.2.4. Stirring diameter of agitator

(1) Effect of stirring diameter on central region in storage tank

The temperature and velocity distributions after 2 h of heating at different D are illustrated in Fig. 36. Upon comparing the velocity and temperature fields shown in Fig. 36, it can be observed that an increase in D leads to a higher proportion of high-speed crude oil in the direction of the agitator, an overall increase in velocity within the computational domain, a more regular distribution of the velocity field, and a wider range of stirring influence. With the effect of impact flow, larger D result in a more pronounced enhancement of heat transfer, thereby improving the temperature distribution within the computational domain. The low temperature region at junctions between different boundaries experiences an enhanced impact effect with increasing D, leading to elevated temperature and reduced coverage within these regions. Overall temperature and uniformity of temperature distribution are also improved as well. For the sections at $X = -4.8$ m, -1.6 m, 1.6 m and 4.8 m, the average temperature in $X = -4.8$ m is always the highest and that in $X = 4.8$ m is always the lowest. With the increase of D from 400 mm to 600 mm, the temperature difference between $X = \pm 4.8$ m increases from 0.01 °C to 0.06 °C. It indicates that increasing D can increase the average temperature in each section along the direction of agitator, which is also evident from contours shown in Fig. 37.

As can be seen from Fig. 37, a large vortex is still formed in center region and its coverage gradually increases with the increase of D. The crude oil covered by the central vortex has great fluidity and the temperature is high. Comparing the temperature field in Fig. 37(a)–(c), it can be seen that when D increases from 400 mm to 500 mm, the coverage of the low temperature region at the boundary junction increases, the reason for this can be explained by the velocity field in Fig. 37(d)–(f). When D is small, some small vortices spontaneously form above the agitator, thereby enhancing flow and heat transfer. However, as D increases to 500 mm, the coverage of the vortex in the center increases and the small vortices in the region above the agitator disappear, resulting in the velocity field in this region mainly affected by the vortex in the center. Due to the limited range of vortex effects, the fluidity of crude oil in this

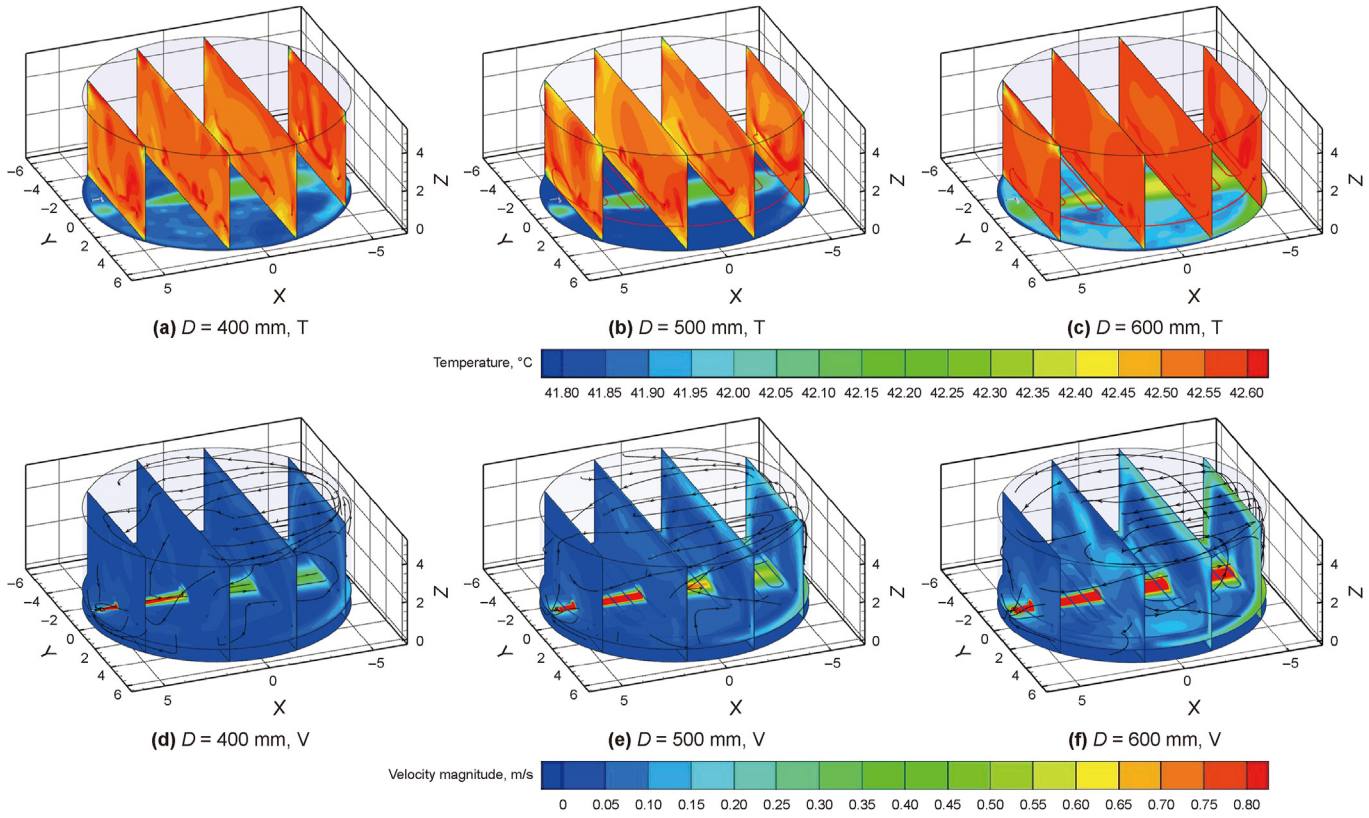

Fig. 36. Effect of stirring diameter on three-dimensional temperature and velocity fields ($t = 2$ h).

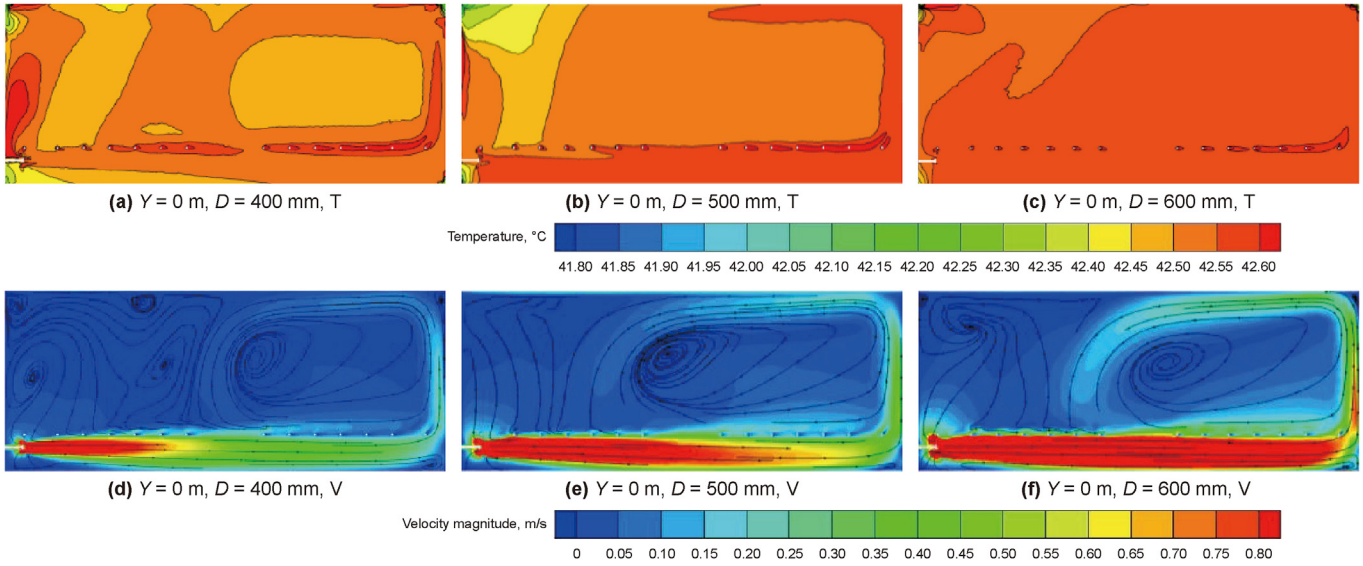

Fig. 37. Effect of stirring diameter on temperature and velocity fields in $Y = 0$ m ($t = 2$ h).

region is poor and heat exchange occurs infrequently, resulting in lower temperature. When D increases to 600 mm, the coverage of the vortex at center is further expanded, which induces a reverse vortex at the boundary junction. This phenomenon enhances heat transfer above the agitator and reduces the coverage of low temperature regions. Therefore, the temperature and velocity distribution in the vicinity of the lower boundary and its surroundings are provided. As shown in Fig. 38(a)–(f), $Z = 0.65$ m denotes the location of the agitator, where a significant coupling characteristics between heat transfer and flow is observed. Upon collision with the boundary, two vortices emerge on both sides of the impact flow, resulting in low temperature at these regions. The proportion of high-speed crude oil in the direction of agitator gradually increases with the increase of D, while the vortices gradually approach the agitator along the side boundary and decrease in size. The high temperature region basically coincides with the trajectory of

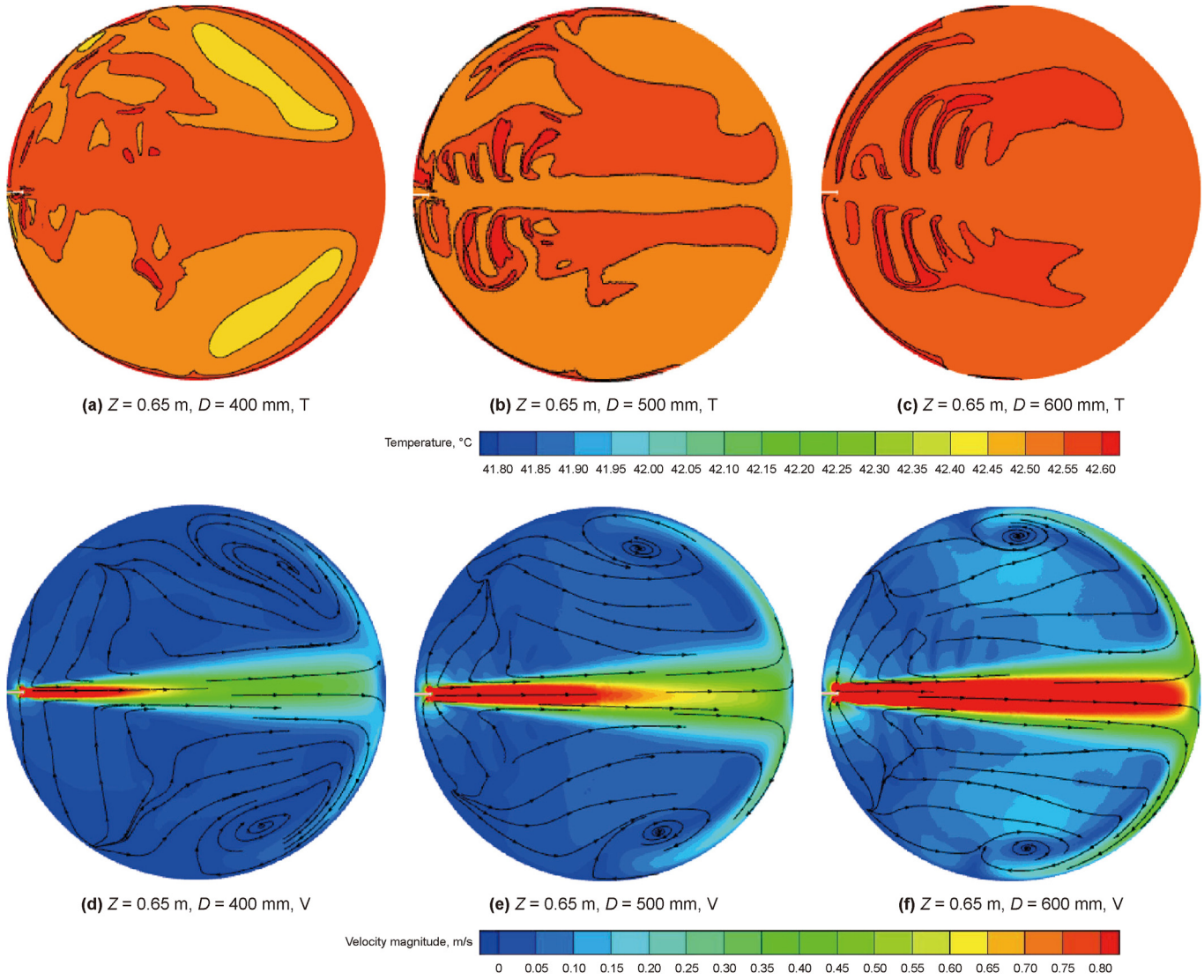

Fig. 38. Effect of stirring diameter on temperature and velocity fields in $Z = 0.65$ m ($t = 2$ h).

impact flow, and this phenomenon is more obvious with the increase of D.

Fig. 39(a) and (b) shows that the increase in D can increase the average crude oil velocity and temperature. The increase in D enhances the coverage of stirring effect and also increases the fluidity of crude oil in computational domain. With the increase of D, the average velocity after stabilization are 0.039 m/s, 0.073 m/s and 0.119 m/s, respectively. After 2 h of heating, the average crude oil temperature are 42.575 °C, 42.586 °C and 42.599 °C, respectively, and the heating rates are 0.288 °C/h, 0.293 °C/h and 0.300 °C/h, respectively. Increasing D also significantly increases the average velocity and improves fluidity for the crude oil, and enhances heat transfer between the crude oil.

(2) Effect of stirring diameter on key region in storage tank

① Effect of stirring diameter on topwall and basewall of storage tank

The temperature distribution in the upper boundary at different D is illustrated in Fig. 40. With an increase in D, significant changes occur in both the overall temperature and temperature uniformity within the upper boundary, while the temperature surrounding the upper boundary remains low. In the inner region of the upper boundary, when D is 400 mm and combined with the velocity field at $Y = 0$ m shown in Fig. 37, due to reduced stirring effects, crude oil flow near the upper boundary relies on weak natural convection resulting in infrequent heat exchange. Consequently, lower temperature region and uneven crude oil distribution are observed within this region. However, when D increases to 500 mm, the stirring effect is enhanced, leading to improved fluidity of crude oil in the upper boundary. This results in increased heat exchange and accumulation of heat in the region opposite to the agitator, thereby increasing overall temperature and temperature uniformity. Furthermore, when D is 600 mm, a higher accumulation of heat occurs in the region opposite to the agitator, leading to elevated temperature in this area. However, a small vortex forms at the upper boundary above the agitator, resulting in weakened heat transfer within the vortex and subsequently causing a decrease in temperature within this specific region. The temperature uniformity in whole upper boundary decreases and the temperature evolves into a both-ends distribution. For topwall of the actual tank, D that too small or too large can adversely affect the temperature and temperature uniformity of crude oil at the topwall of the tank, potentially causing the safety accidents. Reasonable D is of certain

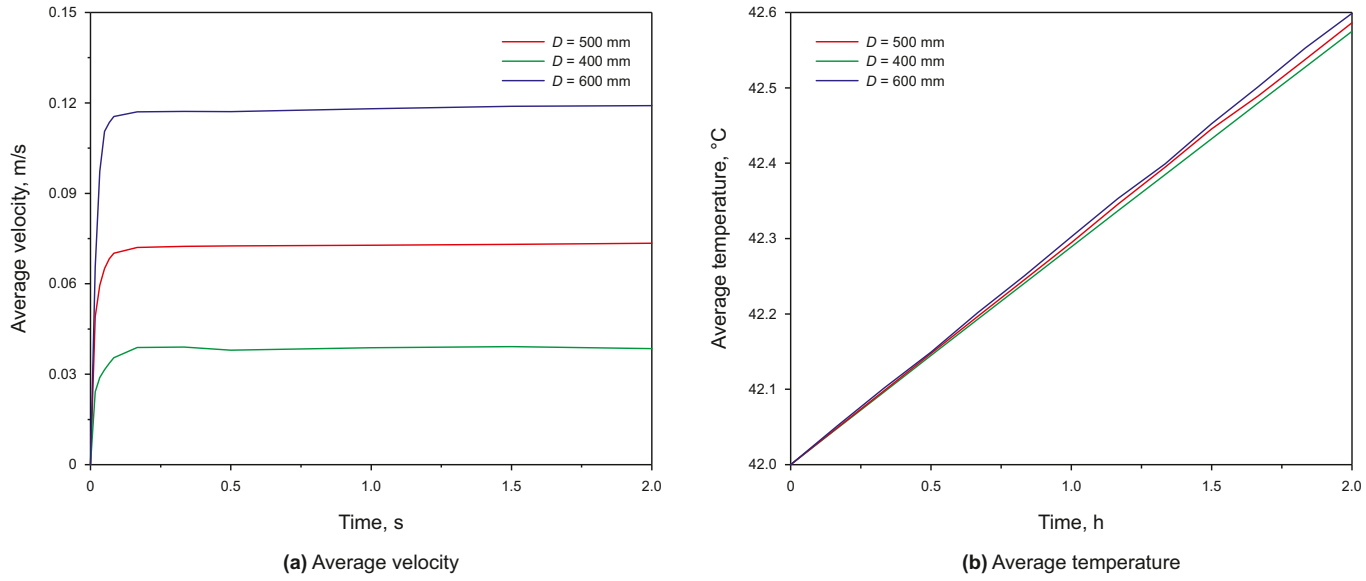

Fig. 39. Effect of stirring diameter on average velocity and temperature.

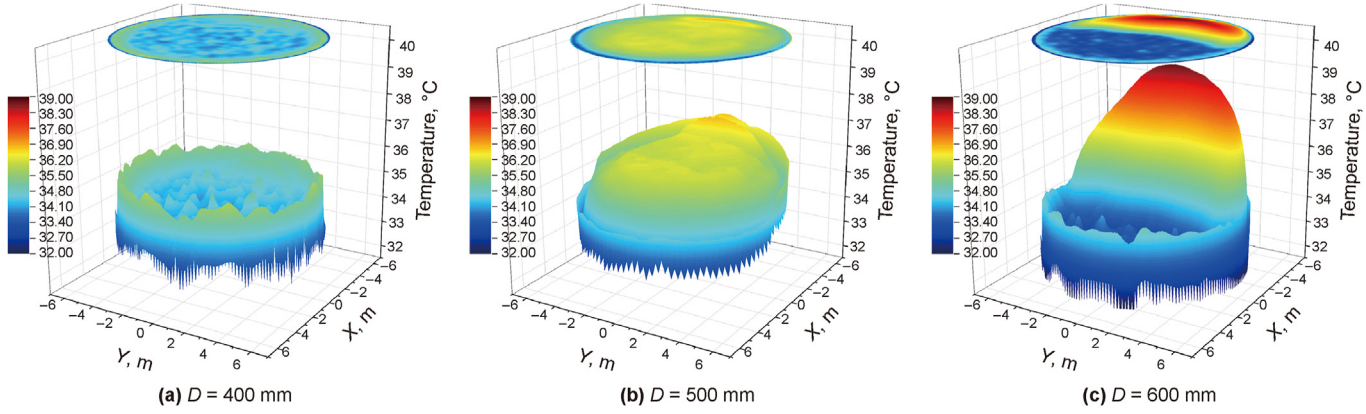

Fig. 40. Effect of stirring diameter on temperature field in upper boundary (t = 2 h).

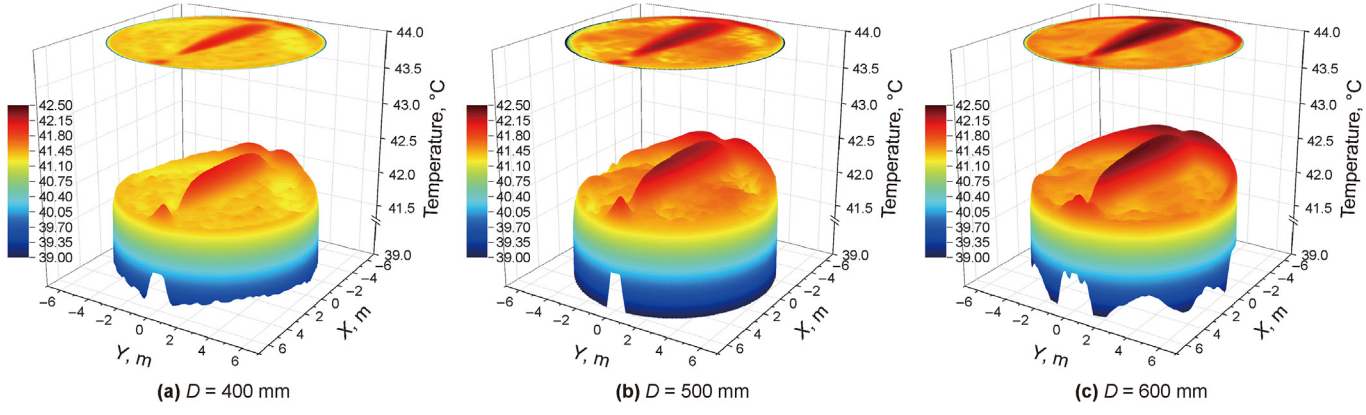

Fig. 41. Effect of stirring diameter on temperature field in lower boundary (t = 2 h).

significance for the safe operation of crude oil storage tank.

Fig. 41 shows the temperature distribution in lower boundary at different D. As a whole, with the synergy of heating and stirring, crude oil temperature in the direction of agitator is high and that on both sides of the stirring direction is low. The impact action takes away more heat and the temperature is high along the stirring direction under the stirring effect. The temperature of central region is always high and shows an upward trend with the increase of

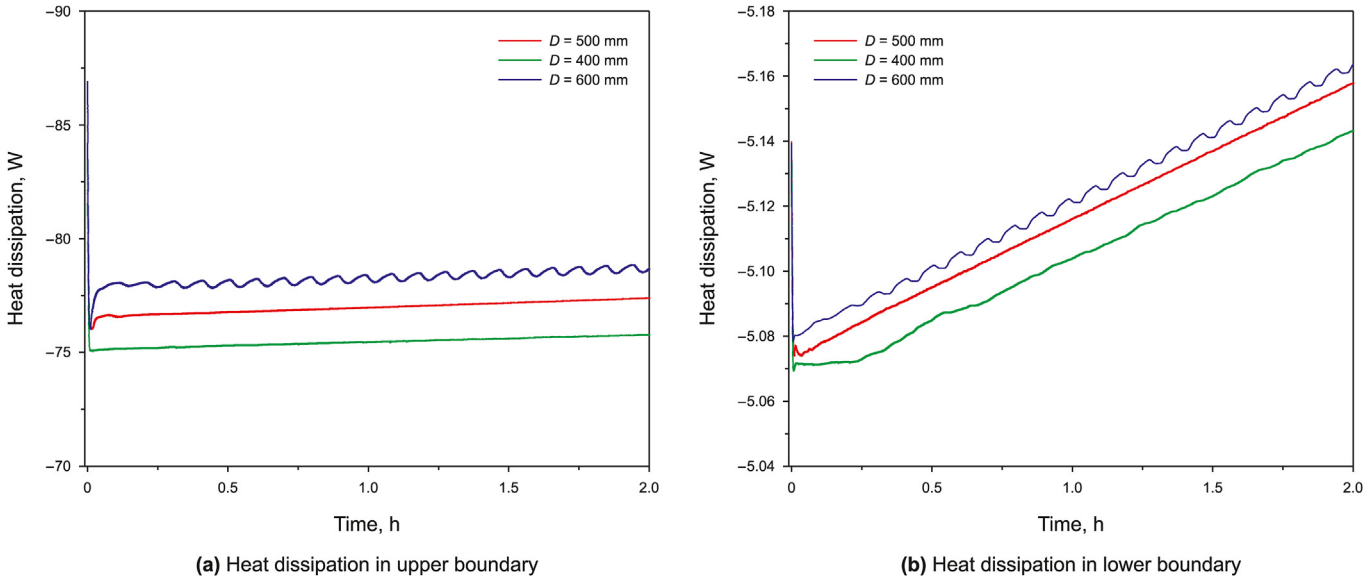

Fig. 42. Effect of stirring diameter on heat dissipation through boundaries.

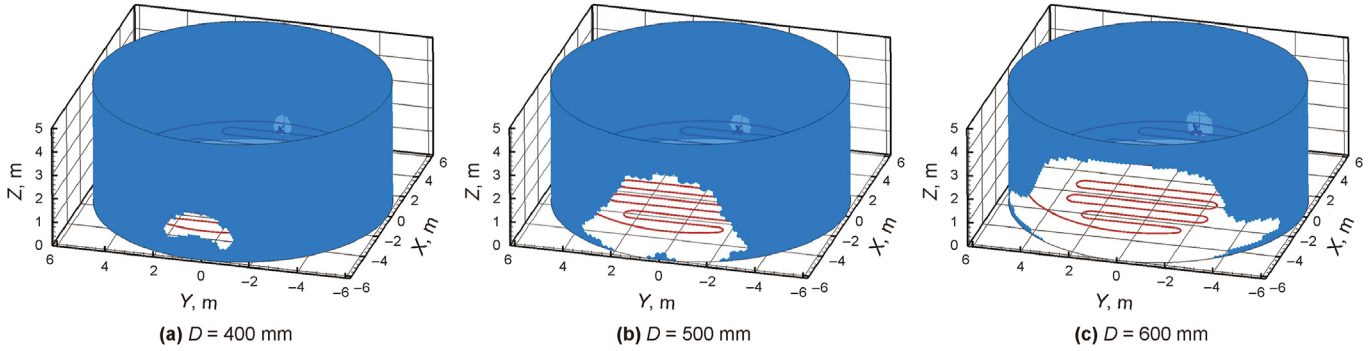

Fig. 43. Low-temperature region distribution at different stirring diameters (t = 2 h).

D. Due to the increase of the overall velocity, it promotes the heat transfer and flow and increases crude oil temperature in the region on both sides of the stirring direction. The overall temperature uniformity in lower boundary gradually increases. For basewall of the actual tank, when D is small, the low temperature region and gelled oil of uneven height are formed at the basewall, the gelled oil could affect normal delivering and receiving operation for storage tank. In the upper and lower boundaries, the crude oil located on the opposite side of agitator has a higher temperature and greater fluidity. Proper installation positioning of the agitator and moderate D are beneficial to delivering and receiving operations for crude oil.

Fig. 42(a) and (b) illustrates the heat dissipation at the upper and lower boundaries, respectively, under varying D. As D increases, there is a gradual rise in heat dissipation with average growth rates of 1.9% and 0.19% for the upper and lower boundaries, respectively. The temporal variation in heat dissipation is consistent with that shown in Fig. 18.

② Effect of stirring diameter on sidewall of storage tank

It can be seen from Fig. 43 that the coverage of the low-temperature region decreases significantly with the increase of D. The volume of low-temperature region decreases from 48.89 m^3 to 12.02 m^3 and the average temperature of it also increases from 36.06 °C to 37.34 °C. The gelled oil is effectively eliminated in the side boundary located on the opposite side of the agitator, significantly improving the low-temperature region in that area. Proper installation positioning of the agitator and moderate D can effectively eliminate gelled oil near both the oil-inlet and oil-outlet, ensuring safe operation during crude oil delivery and receiving.

The topwall, sidewall and basewall of the crude oil storage tank are the accident-prone low temperature key region. As τ increases from 200 rpm to 500 rpm, D increases from 400 mm to 600 mm, the average temperature in the low-temperature region increases by 1.75 °C and 1.28 °C, respectively, and the volume in the low-temperature region decreases by 57.01 m^3 and 36.87 m^3, respectively. The increase of θ_1 and θ_2 can change the distribution position of low-temperature region, but the effect on the average temperature and volume in the low-temperature region is small, and the change rate is within 1.5%. Moderate τ and D, as well as small θ_1 and θ_2 can decrease the distribution of low temperature region and improve the temperature field uniformity at the topwall and basewall of the tank. The temperature on the opposite region of the agitator is higher and the fluidity of crude oil in this region is greater under different stirring parameters. The oil-inlet and oil-outlet should be located on the opposite side of agitator position to ensure the safe operation of delivering and receiving for crude oil.

4.3. Comprehensive evaluation for effect of different stirring parameters on heat transfer characteristics

4.3.1. Comprehensive evaluation for effects of heat transfer characteristics

The influence of different stirring parameters on the temperature are analyzed. In order to evaluate the effect of heat transfer during mechanical stirring and tubular heating, the field synergy theory is introduced (Guo, 2000). The field synergy theory shows that the angle between velocity vector and temperature gradient is mainly used to characterize the effect of heat transfer during heating process (Leng et al., 2009; Hou et al., 2022). Due to the stirring effect, the temperature field distribution is relatively uniform and the temperature gradient is small, so the Temperature-Velocity synergy angle can not change obviously. Meanwhile, the stirring effect makes the overall fluidity of the crude oil great, the flow in some region is violent and the pressure gradient between crude oil is large, and the calculated Pressure-Velocity synergy angle (later referred to as synergy angle β) changes greatly. This synergy angle indicates the magnitude of the flow resistance of crude oil (Tong et al., 2022), the larger the synergy angle, the greater the flow resistance, and the greater the degree of fluid kinetic energy loss. At the same time, the purpose of installing the agitator in the tank is to improve the fluidity of crude oil, but excessive fluidity will correspondingly increase the energy consumption. Considering the actual economy of oilfield production, the analysis of this synergy angle has certain practical significance (Liu and Liu, 2013; Zhang and Zhang, 2017).

In order to comprehensively evaluate the effect of mechanical stirring, in this paper, the synergy angle (β), average temperature ($\overline{T}$), temperature variance of crude oil (σ^2) and heating efficiency of the heater (η) are used as the heat transfer evaluation indices to evaluate the effect of heat transfer in the computational domain. The equations for β, σ^2 and η are calculated by Eqs. (21)–(23).

Fig. 44(a) shows the effect of different stirring parameters on β at 2 h. Under mechanical stirring, due to the existence of viscosity, the high-speed crude oil and the nearby low-speed crude oil are affected by the internal frictional resistance, and the collision between the crude oil and the boundary can cause the momentum brought from the agitator to be partially converted into collision loss and power consumed by viscosity. The wider the β, the greater momentum loss of crude oil. With the increase of different stirring parameters, β increases, the variation range of each β is different. With the increase of τ and D, the stirring effect is enhanced and the

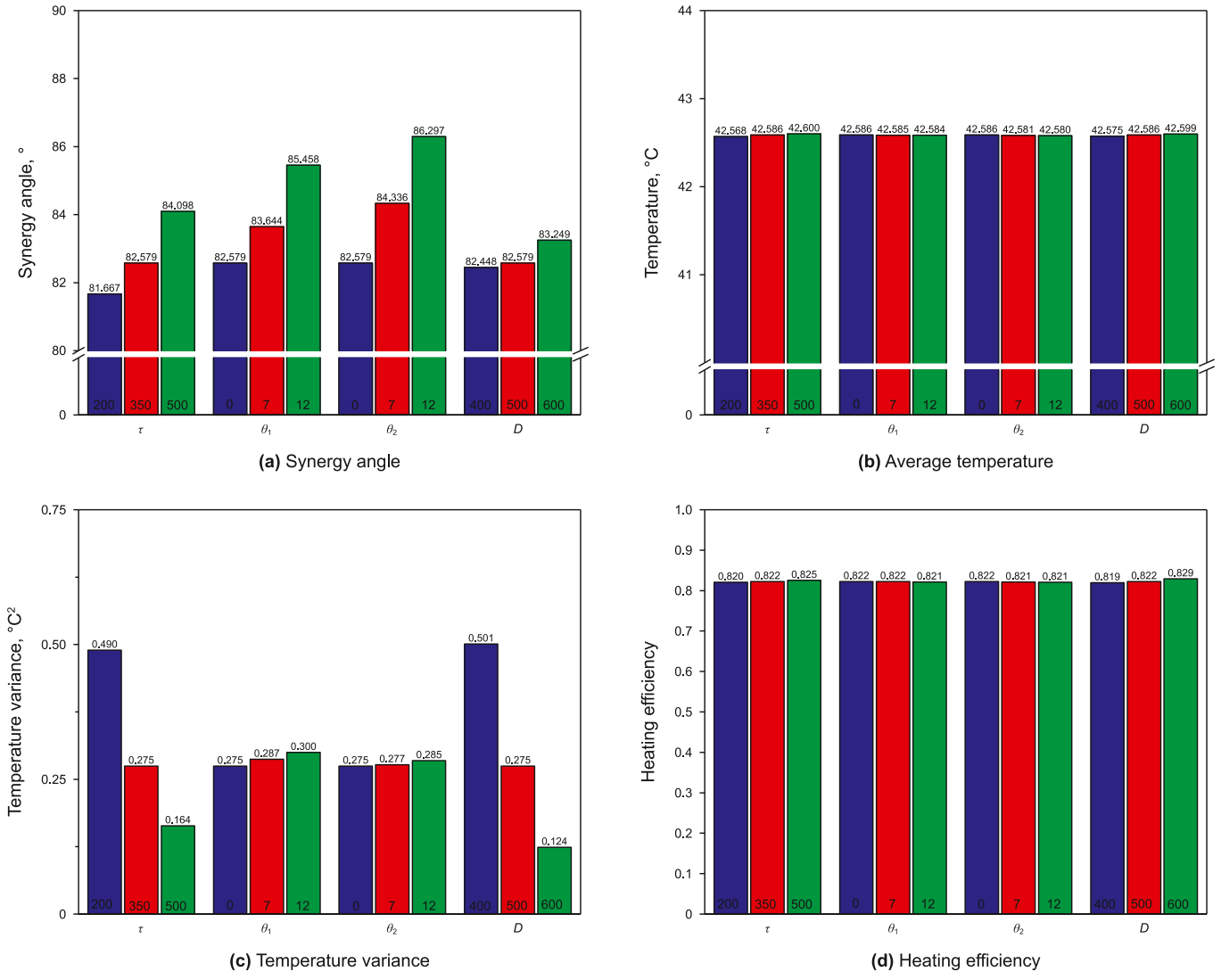

(a) Synergy angle **(b)** Average temperature

(c) Temperature variance **(d)** Heating efficiency

Fig. 44. Effect of stirring parameters on heat transfer evaluation indices.

velocity of crude oil increases, the frictional resistance between crude oil with different velocity increases, the momentum loss and β increase, and the average growth rates of β remain at 1.48% and 0.49%, respectively. For the deflection of agitator, the original velocity field trajectory of crude oil changes and the chaos of velocity field increases, the overall frictional resistance intensifies so that the momentum loss of crude oil increases. β increases with the increase of deflection angle, and the average growth rates of β are 1.73% and 2.23% for θ_1 and θ_2, respectively. Fig. 44(b) shows the effect of different stirring parameters on $\overline{T}$ at 2 h. Since the temperature of heating tube is constant, different stirring parameters only change the heat transfer path and cannot make the crude oil get more heat from heating tube. So the above four stirring parameters have little influence on $\overline{T}$ in the computational domain. With the increase of τ and D, the stirring intensity and overall velocity increases, although β increases, the fluidity can still increase, which promotes heat transfer in the computational domain. For τ and D, $\overline{T}$ shows an upward trend and increases by more than 0.01 °C. When the agitator deflects, with the increase of deflection angle, β and the momentum loss increase, while the stirring intensity remains unchanged, and fluidity of the crude oil decreases. It results in a weakened heat transfer within the computational domain and $\overline{T}$ shows a downward trend. For θ_1 and θ_2, the average decrease in $\overline{T}$ are 0.001 °C and 0.003 °C, respectively. Greater fluidity can improve the heat transfer for crude oil. Fig. 44(c) shows the effect of different stirring parameters on σ^2 at 2 h. σ^2 represents the temperature uniformity of crude oil, the smaller σ^2, the more uniform temperature field. Different stirring parameters have different effects on σ^2. With the increase of τ and D, the fluidity is improved so that the crude oil with higher temperature can be dispersed to a wider range in the computational domain. The heat exchange between crude oil at different temperature improves the temperature uniformity, which decreases σ^2 with average reduction rates of 42.18% and 50.03%, respectively. With the increase of deflection angle, crude oil fluidity decreases, which decreases the heat exchange, and σ^2 increases slightly. For θ_1 and θ_2, the average growth rates of σ^2 are 4.52% and 1.78%, respectively. Fig. 44(d) shows the effect of different stirring parameters on η at 2 h. It can be seen that the overall η does not change much. With the increase of τ and D, $\overline{T}$ increases, η are improved with average growth rates of 0.25% and 0.5%, respectively. However, with the increase of θ_1 and θ_2, due to the decrease in crude oil fluidity, the heat transfer is weakened, $\overline{T}$ decreases and η decreases slightly. For θ_1 and θ_2, the average reduction rates of η are 0.04% and 0.07%, respectively.

For the above result, it can be seen that different stirring parameters have different effects on each evaluation index. The increase in stirring rate (τ) and diameter (D) can improve the fluidity of crude oil and enhance the heat transfer of overall storage tank, but the increase in horizontal (θ_1) and vertical angle (θ_2) of agitator reduce the fluidity of crude oil and have no obvious effect on overall heat transfer. However, the relationship between them cannot be fully indicated by qualitative description alone. So the grey relational analysis is further used to quantitatively rank and clarify the importance of different stirring parameters.

4.3.2. Order of importance for different stirring parameters

To further explore the order of importance for different stirring parameters on heat transfer evaluation indices β, $\overline{T}$, σ^2 and η under synergy of heating and stirring, the grey relational analysis is introduced (Deng, 1982; Mu and Zhang, 2008; Sun et al., 2018b). In order to carry out the grey relational analysis, the reference sequences are taken as the column and the comparison sequences are taken as the row, the following matrix (Eq. (24)) is first established. Take the synergy angle (β) in the heat transfer evaluation indices as an example:

$$A=\begin{pmatrix} a_{1,0} & a_{1,1} & \cdots & a_{1,m} \\ a_{2,0} & a_{2,1} & \cdots & a_{2,m} \\ \vdots & \vdots & \ddots & \vdots \\ a_{n,0} & a_{n,1} & \ldots & a_{n,m} \end{pmatrix} \tag{24}$$

$a_{j,0}$ is the reference sequences, represents the value of synergy angle, $j = 1, 2, \cdots, n$. $a_{j,i}$ is the comparison sequences, represents different stirring parameters, $i = 1, 2, \cdots, m$.

Due to the difference in orders of magnitude between the heat transfer evaluation indices, it is necessary to use dimensionless processing in reference sequences and comparison sequences. The new matrix $a'_{j,i}$ obtained after dimensionless is calculated to obtain the difference sequences between the reference sequence and the comparison sequence. Then the minimum and the maximum ranges are obtained in $a'_{j,i}$, and the relational degree between different stirring parameters and the synergy angle are obtained. The equations for dimensionless, difference sequences, minimum and maximum ranges, relational degree are shown in Eqs. (25)–(28):

$$a'_{j,i}=\frac{a_{j,i}-\min\limits_{k}(a_{k,i})}{\max\limits_{k}(a_{k,i})-\min\limits_{k}(a_{k.i})}\ (i=0,1,\ldots,m;\ k=1,2,\ldots,n) \tag{25}$$

$$\Delta_{j,i}=|a_{j,0}-a_{j,i}|(i=1,2,\cdots,m;\ j=1,2,\cdots,n) \tag{26}$$

$$\begin{cases} \Delta(min)=\min\limits_{i}\left(\min\limits_{j}|a_{j,0}-a_{j,i}|\right) \\ \Delta(max)=\max\limits_{i}\left(\max\limits_{j}|a_{j,0}-a_{j,i}|\right) \end{cases} (i=1,2,\cdots,m;j=1,2,\cdots,n) \tag{27}$$

$$L_{j,i}=\frac{\Delta(min)-\rho\Delta(max)}{|a_{j,0}-a_{j,i}|+\rho\Delta(max)} \tag{28}$$

Based on grey relational analysis, the relational degree of different stirring parameters with the evaluation indices in heating process are quantitatively calculated and their influence are compared. The relational degree of different stirring parameters with β, $\overline{T}$, σ^2 and η are obtained, as shown in Fig. 45.

The relational degree indicates the influence of different stirring parameters on each heat transfer evaluation indices. The greater the relevancy, the greater the impact. As can be seen from Fig. 45, relational degree of different stirring parameters with β, $\overline{T}$, σ^2 and η are different. In the initial stage of stirring and heating, the unstable flow can lead to a large fluctuation of the relational degree. When the stirring and heating are at 0.5 h, the relational degree tends to be stable and the amplitude of fluctuation slows down. The relational degree between τ and heat transfer evaluation indices are the largest, and relational degree between D and the evaluation indices are the least. Due to the fluctuation of relational degree between θ_1 and θ_2 at different times, it is difficult to intuitively distinguish the magnitude of each relational degree. In order to clarify the relational degree between different stirring parameters and heat transfer evaluation indices, the average relational degree of different stirring parameters with β, $\overline{T}$, σ^2 and η are calculated

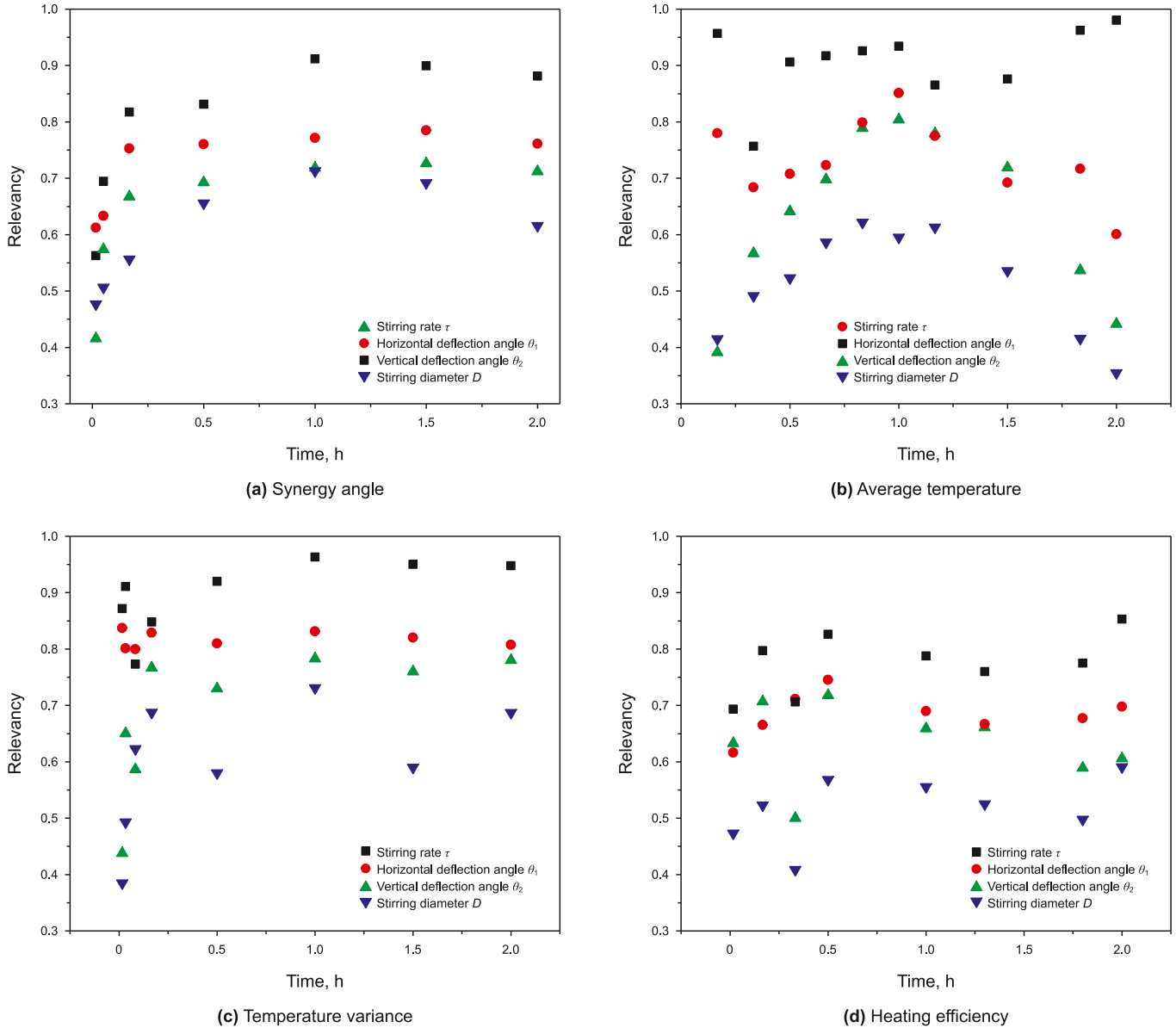

Fig. 45. Effect of different stirring parameters on relational degree.

Table 5
Relational degree of different stirring parameters with evaluation indices.

Stirring parameters	β	$\overline{T}$	σ^2	η	Order
τ	0.799	0.908	0.898	0.774	1
θ_1	0.721	0.732	0.817	0.683	2
θ_2	0.643	0.636	0.686	0.634	3
D	0.602	0.515	0.597	0.528	4

according to the grey correlation analysis, as shown in Table 5. The average relational degree are used as the criterion to evaluate the importance of different stirring parameters, the order: $\tau>\theta_1>\theta_2>D$. This means that in order to improve the heat transfer performance of the crude oil in storage tank, stirring rate (τ) can be increased first, followed by horizontal angle (θ_1), vertical angle (θ_2) and stirring diameter (D) in order of importance of different stirring parameters.

The importance of different stirring parameters has certain practical significance for clarifying the core factors affecting the effect of mechanical stirring and making installation scheme of agitator. However, from the perspective of practical engineering, in order to facilitate the adjustment of the installation scheme of agitator in storage tank, it is necessary to establish the quantitative relationship between different stirring parameters and evaluation indices to guide practical engineering more directly.

4.3.3. Multiple regression analysis

To quantitatively describe the influence of different stirring parameters on each heat transfer evaluation index, t (in h), τ (in rpm), D (in mm), θ_1 and θ_2 (in °) are taken as independent variables, β (in °), $\overline{T}$ (in °C), σ^2 (in °C^2) and η (in %) are used as dependent variables, the relationships between independent variables and dependent variables are obtained by multiple regression analysis. Based on the multiple regression theory, in order to reasonably and accurately express the influence of stirring parameter on heat transfer evaluation indices, the regression equation is established,

Table 6
Multiple regression equations.

	Multiple regression equations	R^2
β	$\beta = e^{3.376}t^{0.012}\tau^{0.232}D^{0.113}\cos\theta_1^{-1.229}\cos\theta_2^{0.617}$	0.83
$\overline{T}$	$\overline{T} = 41.855 + 0.256t + 5.75\times10^{-5}\tau + 4.72\times10^{-5}D + 0.18\cos\theta_1 + 0.02\cos\theta_2$	0.86
σ^2	$\sigma^2 = e^{23.048}t^{-0.025}\tau^{-2.973}D^{-1.003}\cos\theta_1^{-5.161}\cos\theta_2^{-4.227}$	0.82
η	$\eta = e^{-0.71}t^{0.001}\tau^{0.12}D^{-0.025}\cos\theta_1^{0.075}\cos\theta_2^{0.035}$	0.84

such as Eq. (32). To ensure the high accuracy of the regression equations, the values of deflection angle in all the regression equations are represented by their corresponding values of cosine. At the same time, due to the synergy angle, heating efficiency and temperature variance fluctuate greatly with time, and the standard form for the regression equation corresponding to the above evaluation indices is rewritten into logarithmic form (Tang et al., 2024). The goodness of fit is used to evaluate the degree of fit of the regression equations, and the closer R^2 is to 1, the higher the accuracy of the regression equation is reached. The standard form of the regression equation (for temperature), the logarithmic form of the regression equation (for synergy angle, heating efficiency, and temperature variance), the simplified logarithmic form and the goodness of fit of the regression equation are shown in Eqs. (29)–(32).

$$y_i = a_0 + a_1\cdot t + a_2\cdot\tau + a_3\cdot D + a_4\cdot\cos\theta_1 + a_5\cdot\cos\theta_2 \tag{29}$$

$$\ln y_i = a_0 + a_1\ln t + a_2\ln\tau + a_3\ln D + a_4\ln(\cos\theta_1) + a_5\ln(\cos\theta_2) \tag{30}$$

$$y_i = e^{a_0}\cdot t^{a_1}\cdot\tau^{a_2}\cdot D^{a_3}\cdot(\cos\theta_1)^{a_4}\cdot(\cos\theta_2)^{a_5} \tag{31}$$

$$R^2 = 1 - \frac{\sum(\widehat{y}_i - y_i)^2}{\sum(y_i - \overline{y})^2} \tag{32}$$

$\overline{y}, \widehat{y}_i, y_i$ are the average value of each heat transfer evaluation index, the calculated value by the regression equations, and the actual value of evaluation indices. Multiple regression equations are shown in Table 6.

The coefficients of deflection angle in regression equations correspond to their cosine values, making it challenging to visually judge the relationship between coefficients for different stirring parameters. However, the absolute value of coefficient for τ is consistently greater than that for D in all equations, and the absolute value of coefficient for θ_1 is also greater than that for θ_2. From the perspective of heat transfer performance, establishing quantitative equations with a high degree of fit can quantify the range of adjusting the stirring parameters, provide guidance and basis for adjusting stirring parameters and improving heating efficiency in the tanks. Nevertheless, considering energy utilization and loss, comprehensively describing the effects of different stirring parameters and optimizing them requires taking into account thermodynamic characteristics in crude oil storage tank systems under the synergy of heating and stirring.

4.4. Thermodynamic optimization on different stirring parameters for energy utilization efficiency in storage tank

The thermodynamic theory is used to analyze the above 9 cases. Bejan (1995) got the expression of entropy generation in the process of flow and heat transfer, and introduced the entropy generation minimization into the optimal design of thermal systems. The optimization goal of entropy generation minimization is essentially to minimize the power capability loss of the system. In the optimal design of heat transfer systems and power-heat conversion systems, the entropy generation minimization theory has been widely used because it can decrease the irreversibility for the system (Ibanez and Cuevas, 2010; Chen et al., 2018; Kashyap and Dass, 2018). For crude oil storage tank system, the entropy generation of crude oil is due to irreversibility in thermal processes. There are two types of entropy generation, namely entropy generation owing to heat transfer ΔS^1_{gen} and viscous fluid flow ΔS^2_{gen}, they are calculated by Eqs. (33) and (34), total entropy generation ΔS^{tot}_{gen} is calculated as Eq. (35) (Duan et al., 2014).

$$\Delta S^1_{gen,i} = \frac{\lambda_{oil}}{T^2}\left[\left(\frac{\partial T}{\partial x}\right)^2 + \left(\frac{\partial T}{\partial y}\right)^2 + \left(\frac{\partial T}{\partial z}\right)^2\right] \tag{33}$$

$$\Delta S^2_{gen,i} = \frac{\mu}{\overline{T}}\left\{2\left[\left(\frac{\partial\overline{u}}{\partial x}\right)^2 + \left(\frac{\partial\overline{v}}{\partial y}\right)^2 + \left(\frac{\partial\overline{w}}{\partial z}\right)^2\right]\right\} + \left(\frac{\partial\overline{u}}{\partial y} + \frac{\partial\overline{v}}{\partial x}\right)^2 + \left(\frac{\partial\overline{u}}{\partial z} + \frac{\partial\overline{w}}{\partial x}\right)^2 + \left(\frac{\partial\overline{v}}{\partial z} + \frac{\partial\overline{w}}{\partial y}\right)^2 \tag{34}$$

$$\Delta S^{tot}_{gen} = \sum_{i=1}^{n}\left(\Delta S^1_{gen,i}\cdot V_i\right) + \sum_{i=1}^{n}\left(\Delta S^2_{gen,i}\cdot V_i\right) \tag{35}$$

where $\overline{T}$ is crude oil average temperature at 2 h, °C. $\overline{u}, \overline{v}, \overline{w}$ are the average value of velocity components in X, Y, and Z directions, m/s, respectively. $\Delta S^1_{gen,i}$, $\Delta S^2_{gen,i}$ are the entropy generation caused by heat transfer and viscous fluid flow in ith grid, J/K.

The entropy generation caused by heat transfer and viscous fluid flow exhibits variations under different stirring parameters, as evident from Table 7. Changes in the stirring parameters influence the distribution of velocity field in crude oil, thereby altering the entropy generation induced by viscous fluid flow ΔS^2_{gen}. Simultaneously, due to the significant coupling characteristics between flow and heat transfer that impact heat transfer, the temperature field and the entropy production caused by heat transfer ΔS^1_{gen} also change. Consequently, the total entropy generation also varies under different stirring parameters. Compared with Case 1, the changes in the stirring parameters could lead to an increase in total entropy generation, with a minimum relative change of 1.39% (Case 2) and a maximum relative change of 18.53% (Case 9) in total entropy generation. When τ = 350 rpm, $\theta_1 = \theta_2 = 0°$, D = 500 mm (Case 1), the total entropy generation is the least. According to thermodynamics theory, in a closed system, entropy production is a measure of the increase in entropy of a system over an irreversible process. The process of energy conversion and flow of matter is always accompanied by an increase in entropy. The entropy generation represents the irreversible loss in the whole system, and the less the entropy production, the less the irreversible loss in the system. The structure with less irreversible loss has better heat transfer performance (Zhao et al., 2021b). The structure of agitator

Table 7
Entropy generation under different stirring parameters.

	Case	Entropy generation caused by heat transfer ΔS^1_{gen}, J/K	Entropy generation caused by viscous fluid flow ΔS^2_{gen}, J/K	Total entropy generation of crude oil ΔS^{tot}_{gen}, J/K	Relative change in total entropy production
	1	89545	95757	185302	0
τ	2	111884	76032	187916	1.39%
	3	80142	121688	201830	8.19%
θ_1	4	88137	116701	204838	9.54%
	5	88662	123554	212216	12.68%
θ_2	6	106739	108351	215090	13.85%
	7	107688	108692	216380	14.36%
D	8	109979	86938	196917	5.90%
	9	79304	148153	227457	18.53%

with optimal heat transfer performance and flow can be found (Zhao et al., 2017b; Ji et al., 2020) with the optimization method based on the entropy generation minimization (Bejan, 1982). In conclusion, when $\tau = 350$ rpm, $\theta_1 = \theta_2 = 0°$, $D = 500$ mm, the total entropy generation is the least, the irreversible loss in the system is the least, and the heat transfer performance of the storage tank system is the optimal under synergy of heating tube and mechanical stirring.

5. Conclusions

Considering the changes of physical and chemical properties of crude oil before and after the temperature at the anomaly point, as well as the influence of wax crystal precipitation on the specific heat of crude oil during the cooling process, the heat transfer process under the synergistic effect of tubular heating and mechanical stirring under different stirring parameters is studied. Grey correlation analysis, multiple regression analysis and entropy yield minimization are used for quantitative analysis. The following conclusions are obtained.

(1) For a 1000 m^3 crude oil storage tank, the coupling characteristics of flow and heat transfer are significant. Under the synergy of heating and stirring, changes in stirring rate (τ), horizontal deflection angle (θ_1), vertical deflection angle (θ_2) and stirring diameter (D) would lead to the change in the velocity field for crude oil, and affect the heat transfer path, which in turn can lead to the change in the temperature field.

(2) The topwall, sidewall and basewall of the crude oil storage tank are the accident-prone low temperature key region. As τ increases from 200 rpm to 500 rpm, D increases from 400 mm to 600 mm, the average temperature in the low-temperature region increases by 1.75 °C and 1.28 °C, respectively, and the volume in the low-temperature region decreases by 57.01 m^3 and 36.87 m^3, respectively. The increase of θ_1 and θ_2 can change the distribution position of low-temperature region, but the effect on the average temperature and volume in the low-temperature region is small, and the change rate is within 1.5%. Moderate τ and D, as well as small θ_1 and θ_2 can decrease the distribution of low temperature region and improve the temperature field uniformity at the topwall and basewall of the tank. The temperature on the opposite region of the agitator is higher and the fluidity of crude oil in this region is greater under different stirring parameters. The oil-inlet and oil-outlet should be located on the opposite side of agitator position to ensure the safe operation for delivering and receiving for crude oil.

(3) The relational degree of different stirring parameters with heat transfer evaluation indices (synergy angle, average temperature, temperature variance and heating efficiency) are calculated by grey correlation analysis to rank the importance of different stirring parameters. The average relational degree of different stirring parameters with heat transfer evaluation indices are used as the criterion to evaluate the importance of different stirring parameters, the order: $\tau > \theta_1 > \theta_2 > D$. Subsequently, with the multiple regression analysis, the relationship between different stirring parameters and the heat transfer evaluation indices are quantitatively described by equations. In order to improve the heat transfer performance of crude oil in the storage tank, the stirring parameters with greater importance can be adjusted accurately according to the multiple regression equations and importance of different stirring parameters.

(4) Based on entropy generation minimization, the synergy process of tubular heating and mechanical stirring in crude oil storage tank is optimized. The results show that when $\tau = 350$ rpm, $\theta_1 = \theta_2 = 0°$, $D = 500$ mm, the total entropy generation is the least, the irreversible loss is the least, and the heat transfer performance of crude oil storage tank system is optimal. The research results can provide theoretical guidance for the structural design and operation parameter optimization of agitators in actual crude oil storage tanks.

CRediT authorship contribution statement

Jian Zhao: Writing – review & editing. **Ming-Yu Lei:** Writing – original draft. **Shu-Qi Liu:** Methodology. **Hang Dong:** Visualization.

Declaration of competing interest

There is no conflict of interest.

Acknowledge

This work is supported by the National Natural Science Foundation of China (Grant no. 52304065) and China Postdoctoral Science Foundation (Grant no. 2022MD723759).

References

Bejan, A., 1982. Entropy Generation through Heat and Fluid Flow. Wiley, New York.
Bejan, A., 1995. Entropy Generation Minimization. CRC Press.
BP, 2023. BP Energy-Outlook 2023.
Chala, G.T., Sulaiman, S.A., Japper-Jaafar, A., 2018. Flow start-up and transportation of waxy crude oil in pipelines-A review. J Nonnewton Fluid Mech 251, 69–87. https://doi.org/10.1016/j.jnnfm.2017.11.008.
Chen, X.R., Zhang, Z.F., Jun, X., 2010. Effects of annular electromagnetic stirring processing parameters on semi-solid slurry production. Trans. Nonferrous Metals Soc. China 20, 873–877. https://doi.org/10.1016/S1003-6326(10)60598-5.
Chen, Y.R., 1999. Oil and Gas Storage and Transportation Construction Engineering Manual. China Architecture & Building Press.
Chen, L.G., Zhang, L., Xia, S.J., Sun, F.S., 2018. Entropy generation minimization for

CO_2 hydrogenation to light olefins. Energy 147, 187–196. https://doi.org/10.1016/j.energy.2018.01.050.
Deng, J.L., 1982. The grey control system. J. Huazhong Univ. Sci. Technol. - Med. Sci. 10 (3), 9–18. https://doi.org/10.13245/j.hust.1982.03.002 (in Chinese).
Du, Y.H., Zhang, P., Wang, Y.J., Zhang, J., Yao, S.S., Li, C.Y., 2013. The uniform distribution of SiC particles in an A356-SiC p composite produced by the tilt-blade mechanical stirring. Acta Metall Sin-engl 26, 69–74. https://doi.org/10.1007/s40195-012-0502-9.
Duan, L., Wu, X.L., Ji, Z.L., 2014. Application of entropy generation method for analyzing energy loss of cyclone separator. CIE J. 65 (2), 583–592. https://doi.org/10.3969/j.issn.0438-1157.2014.02.031 (in Chinese).
Fang, X., Zou, H., 2022. Revisiting the preparation of cylindrical polystyrene particles by magnetic stirring. Colloids Surf., A 638, 128308. https://doi.org/10.1016/j.colsurfa.2022.128308.
Fernandes, D.M., Montes, R.H., Almeida, E.S., Nascimento, A.N., Oliveira, P.V., Richter, E.M., Muñoz, R.A., 2013. Storage stability and corrosive character of stabilised biodiesel exposed to carbon and galvanised steels. Fuel 107, 609–614. https://doi.org/10.1016/j.fuel.2012.11.010.
Guo, Z., 2000. Physical mechanism of convective heat transfer and its control: synergy of velocity and heat flow fields. Chin. Sci. Bull. 45 (19), 2118–2122. https://doi.org/10.3321/j.issn:0023-074X.2000.19.020 (in Chinese).
Hou, J.S., Wu, X.L., Chen, K., Dong, Y., 2022. A direct optimization strategy based on field synergy equation for efficient design of battery thermal management system. Int. J. Heat Mass Tran. 184, 122304. https://doi.org/10.1016/j.ijheatmasstransfer.2021.122304.
Ibanez, G., Cuevas, S., 2010. Entropy generation minimization of a MHD (magnetohydrodynamic) flow in a microchannel. Energy 35 (10), 4149–4155. https://doi.org/10.1016/j.energy.2010.06.035.
Ji, L.L., Li, W., Shi, W.D., Chang, H., Yang, Z.Y., 2020. Energy characteristics of mixed-flow pump under different tip clearances based on entropy production analysis. Energy 199, 117447. https://doi.org/10.1016/j.energy.2020.117447.
Kashyap, D., Dass, A.K., 2018. Two-phase lattice Boltzmann simulation of natural convection in a Cu-water nanofluid-filled porous cavity: effects of thermal boundary conditions on heat transfer and entropy generation. Adv. Powder Technol. 29 (11), 2707–2724. https://doi.org/10.1016/j.apt.2018.07.020.
Lei, M.Y., Zhao, J., Wang, H.T., Zhou, X.C., 2024. Effect of mechanical stirring on heat transfer and flow of crude oil in storage tanks under different heating methods. Case Stud. Therm. Eng. 58, 104382. https://doi.org/10.1016/j.csite.2024.104382.
Leng, X.L., Zhang, G.M., Tian, M.C., Cheng, L., 2009. Methods for applying field synergy principle in convection heat exchange. J. Eng. Therm. Energy Power 24 (3), 352–354 (in Chinese).
Li, Y.B., Wei, Z.Y., Li, Y.T., Shen, Q., Lin, Z.Q., 2013. Effects of cone angle of truncated electrode on heat and mass transfer in resistance spot welding. Int. J. Heat Mass Tran. 65, 400–408. https://doi.org/10.1016/j.ijheatmasstransfer.2013.06.012.
Li, Z.X., Li, B., Wang, H., Yang, J.X., Xu, J.X., 2021a. Effect of gas-liquid two-phase macro-mixing on the uniformity of temperature distribution in a top-blown stirred tank using image analysis. Int. J. Therm. Sci. 168, 107083. https://doi.org/10.1016/j.ijthermalsci.2021.107083.
Li, Y.H., Zhao, J., Dong, H., Xi, X.R., 2021b. The role of shearing effect in the evolution of the microscopic behavior of wax crystals. New J. Chem. 45 (23), 10418–10431. https://doi.org/10.1039/D1NJ01407B.
Liu, W., Liu, Z.C., Ma, L., 2012. Physical quantity application of a multi-field synergy principle in the performance evaluation of convective heat transfer enhancement in a tube. Chin. Sci. Bull. 57 (10), 867–874. https://doi.org/10.1007/s11434-012-5062-x (in Chinese).
Liu, J.J., Liu, W., 2013. A numerical study on heat transfer of three-start spirally corrugated tubes. J. Eng. Thermophys. 34 (11), 2128–2131 (in Chinese).
Luo, Y.j., Wu, Z.G., Zhou, L., He, M., Zhang, Z.L., Peng, X.M., Zhang, Z.F., 2020. Effect of electromagnetic stirring position on uniform direct chill casting of large-sized 7005 alloy billet. J. Miner. Met. Mater. Soc. 72, 4665–4673. https://doi.org/10.1007/s11837-020-04362-7.
Mao, Q., Zhang, L., Wu, H., 2016. Numerical simulation on heat transfer characteristics of the storage tank for concentrating solar power plant. Adv. Mech. Eng. 8 (7). https://doi.org/10.1177/1687814016656105.
Mawire, A., 2013. Experimental and simulated thermal stratification evaluation of an oil storage tank subjected to heat losses during charging. Appl. Energy 108, 459–465. https://doi.org/10.1016/j.apenergy.2013.03.061.
Mu, R., Zhang, J.T., 2008. Research of hierarchy synthetic evaluation based on grey relational analysis. Syst. Eng. (10), 125–130. https://doi.org/10.1109/GSIS.2007.4443243.
Roldan-Cruz, C., Garcia-Hernandez, A., Alvarez-Ramirez, J., Vernon-Carter, E.J., 2021. Effect of the stirring speed in the in vitro activity of α-amylase. Food Hydrocolloids 110, 106127. https://doi.org/10.1016/j.foodhyd.2020.106127.
Scholz, P., Keck, C.M., 2015. Nanoemulsions produced by rotor–stator high speed stirring. Int. J. Pharm. 482 (1–2), 110–117. https://doi.org/10.1016/j.ijpharm.2014.12.040.
Seddegh, S., Wang, X.L., Henderson, A.D., 2015. Numerical investigation of heat transfer mechanism in a vertical shell and tube latent heat energy storage system. Appl. Therm. Eng. 87, 698–706. https://doi.org/10.1016/j.applthermaleng.2015.05.067.
Souas, F., Safri, A., Benmounah, A., 2021. A review on the rheology of heavy crude oil for pipeline transportation. Pet. Res 6 (2), 116–136. https://doi.org/10.1016/j.ptlrs.2020.11.001.
Sun, W., Cheng, Q.L., Zheng, A.B., Zhang, T.Y., Liu, Y., 2018a. Research on coupled characteristics of heat transfer and flow in the oil static storage process under periodic boundary conditions. Int. J. Heat Mass Tran. 122, 719–731. https://doi.org/10.1016/j.ijheatmasstransfer.2018.02.010.
Sun, W., Cheng, Q.L., Wang, P.D., Yi, X., 2016. Numerical simulation of steam coil heating process for large floating roof oil tank. Chem. Eng. J. 44 (7), 19–23. https://doi.org/10.3969/j.issn.1005-9954.2016.07.005 (in Chinese).
Sun, G.D., Guan, X., Yi, X., Zhou, Z., 2018b. Grey relational analysis between hesitant fuzzy sets with applications to pattern recognition. Expert Syst. Appl. 92, 521–532. https://doi.org/10.1016/j.eswa.2017.09.048.
Tang, Z.P., Wu, Y., Xiong, S.F., Huang, H., 2024. A mixed geographically weighted regression model with varying-coefficient spatial lag. J. Univ. Chin. Acad. Sci. 41 (3), 345–356. https://doi.org/10.7523/j.ucas.2022.081 (in Chinese).
Tong, Z.X., Li, M.J., Ding, Y., 2022. A field synergy principle of velocity and pressure for flow resistance reduction. J. Enhanc. Heat Transf. 29, 1. https://doi.org/10.1615/jenhheattransf.2022041060.
Wang, R., Bi, S.S., Tian, J., Shen, Y.H., 2023. Analysis of the economic operation of China coastal port crude oil system in the first half of 2023. China Ports (9), 11–12+4. https://doi.org/10.3969/j.issn.1006-124X.2023.09.005 (in Chinese).
Wang, M., Shao, Q.Q., Yang, X.F., Li, J.F., 2020a. Study on influence of inclination of coils on melting process of waxy crude oil in a floating roof tank. CIE J. 71 (5), 2035–2048. https://doi.org/10.11949/0438-1157.20191431 (in Chinese).
Wang, Y.D., Chen, W., Jiang, D.B., Zhang, L.F., 2020b. Effect of the gap between copper mold and solidified shell on the fluid flow in the continuous casting strand with mold electromagnetic stirring. Steel Res. Int. 91 (2), 1900470. https://doi.org/10.1002/srin.201900470.
Wang, M., Li, J.F., Zhang, X.Y., Yu, B., 2017. Numerical study on the temperature drop characteristics of waxy crude oil in a single-plate floating roof oil tank. Pet. Sci. Bull. 2 (2), 267–278. https://doi.org/10.3969/j.issn.2096-1693.2017.02.025 (in Chinese).
Yang, L., Zhao, J., Dong, H., Liu, J.Y., Zhao, W.Q., 2018. Research on temperature profile in a large scaled floating roof oil tank. Case Stud. Therm. Eng. 12, 805–816. https://doi.org/10.1016/j.csite.2018.10.009.
Zhang, Y.Q., Pan, X., Wang, Y.H., Luo, P.C., Wu, H., 2018. Numerical and experimental investigation on surface air entrainment mechanisms of a novel long-short blades agitator. AIChE J. 64 (1), 316–325. https://doi.org/10.1002/aic.15865.
Zhang, Z., Zheng, Y., Jiang, J.Q., Li, C.Y., 2020a. Influence of wastewater mixer setting angle on flow field in sewage treatment pool. J. Drain. Irriga. Mach. Eng. 38 (3), 271–276. https://doi.org/10.3969/j.issn.1674-8530.18.0143 (in Chinese).
Zhang, H.Y., Zheng, Y., Zhang, Z., Mo, X.Y., 2021. Influence of placement angle of sewage mixer on its hydraulic characteristics. J. Drain. Irriga. Mach. Eng. 39 (5), 483–487. https://doi.org/10.3969/j.issn.1674-8530.19.0284 (in Chinese).
Zhang, Q.B., Yuan, F.L., Fu, Y., 2012. Risk analysis and safety countermeasures of the large floating roof tank. J. Safe. Sci. Technol. 8 (6), 134–138. https://doi.org/10.3969/j.issn.1673-193X.2012.06.026 (in Chinese).
Zhang, Y., Yang, T., Zhang, J.B., Lv, B.Y., Cheng, X.S., Fang, Y., 2020b. Laboratory investigation into the evaporation of natural-gas condensate oils: hints for the sanchi oil spill. J. Ocean Univ. China 19, 633–642. https://doi.org/10.1007/s11802-020-4113-1.
Zhang, A.P., Zhang, Y., 2017. Ultrasound effects on improving heat transfer based on field synergy theory. J. Eng. Therm. Energy Power 32 (5), 19–25+134. https://doi.org/10.16146/j.cnki.rndlgc.2017.05.004 (in Chinese).
Zhao, J., Xi, X.R., Dong, H., Wang, Z.H., Zhuo, Z.W., 2022a. Rheo-microscopy in situ synchronous measurement of shearing thinning behaviors of waxy crude oil. Fuel 323, 124427. https://doi.org/10.1016/j.fuel.2022.124427.
Zhao, J., Liu, J.Y., Dong, H., Rong, G.X., 2019a. Numerical study on the static cooling of waxy crude oil in the vault tank. IEEE Access 7, 108850–108865. https://doi.org/10.1109/access.2019.2933036.
Zhao, J., Liu, J.Y., Dong, H., Zhao, W.Q., 2019b. Effect of physical properties on the heat transfer characteristics of waxy crude oil during its static cooling process. Int. J. Heat Mass Tran. 137, 242–262. https://doi.org/10.1016/j.ijheatmasstransfer.2019.03.081.
Zhao, J., Dong, H., Wang, X.L., Fu, X.M., 2017a. Research on heat transfer characteristic of crude oil during the tubular heating process in the floating roof tank. Case Stud. Therm. Eng. 10, 142–153. https://doi.org/10.1016/j.csite.2017.05.006.
Zhao, J., Zhou, X.C., Xia, D., Dong, H., 2023a. Study on influence of mechanical stirring on heat transfer characteristics during jet heating of crude oil storage tank. CIE J. 74 (5), 1982–1999. https://doi.org/10.11949/0438-1157.20230006 (in Chinese).
Zhao, J., Lei, M.Y., Jiang, M.Z., Li, Y.P., Dong, H., 2023b. Effect of mechanical stirring on the tubular heating process of crude oil. Int. J. Heat Mass Tran. 211, 124213. https://doi.org/10.1016/j.ijheatmasstransfer.2023.124213.
Zhao, J., Xi, X.R., Dong, H., Li, Y.H., Jiang, M.Z., 2021a. In situ observation of microscopic motions and the structure dynamic transformation of wax crystals in waxy crude oil subjected to shear. New J. Chem. 45 (37), 17522–17543. https://doi.org/10.1039/D1NJ02292J.
Zhao, J., Li, X.F., Dong, H., Wang, Z.H., 2022b. Rheo-optic in situ synchronous study on the gelation behaviour and mechanism of waxy crude oil emulsions. Petrol. Sci. https://doi.org/10.1016/j.petsci.2022.08.033.
Zhao, Z., Xu, L., Gao, J.M., Xi, L., Li, Y.L., 2021b. A study on the flow and heat transfer characteristics of heat exchanger with cone-Type vortex generators. J. Xi'an Med. Univ. 55 (10), 131–143. https://doi.org/10.7652/xjtuxb202110015 (in Chinese).
Zhao, L.P., Gu, X.T., Wang, R.J., Yang, Z.G., 2017b. Entropy generation analysis and structure optimizationof rectangular finned elliptical tube heat exchangers. J. Therm. Sci. Technol. 16 (4), 337–344. https://doi.org/10.13738/j.issn.1671-8097.2017.04.013 (in Chinese).